Olfactory detection of viruses shapes brain immunity and behavior in zebrafish

Aurora Kraus[1], Benjamin Garcia[1], Jie Ma[2], Kristian J. Herrera[3], Hanna Zwaka[3], Roy Harpaz[3], Ryan Y. Wong[4], Florian Engert[3], Irene Salinas[1*].

Affiliations

[1] Center for Evolutionary and Theoretical Immunology, Department of Biology, University of New Mexico, Albuquerque, NM 87131, USA.

[2] Department of Fish & Wildlife Sciences, University of Idaho, P.O. Box 441136, Moscow, ID 83844-1136, USA.

[3] Department of Molecular and Cellular Biology, Harvard University, 16 Divinity Avenue, Cambridge, MA 02138, USA.

[4] University of Nebraska at Omaha, Department of Biology, 6001 Dodge Street, Omaha, NE 68182; USA.

Correspondence: isalinas@unm.edu

Abstract

Olfactory sensory neurons (OSNs) are constantly exposed to pathogens, including viruses. However, serious brain infection via the olfactory route rarely occurs. When OSNs detect a virus, they coordinate local antiviral immune responses to stop virus progression to the brain. Despite effective immune control in the olfactory periphery, pathogen-triggered neuronal signals reach the CNS via the olfactory bulb (OB). We hypothesized that neuronal detection of a virus

by OSNs initiates neuroimmune responses in the OB that prevent pathogen invasion. Using zebrafish (*Danio rerio*) as a model, we demonstrate viral-specific neuronal activation of OSNs projecting into the OB, indicating that OSNs are electrically activated by viruses. Further, behavioral changes are seen in both adult and larval zebrafish after viral exposure. By profiling the transcription of single cells in the OB after OSNs are exposed to virus, we found that both microglia and neurons enter a protective state. Microglia and macrophage populations in the OB respond within minutes of nasal viral delivery followed decreased expression of neuronal differentiation factors and enrichment of genes in the neuropeptide signaling pathway in neuronal clusters. Pituitary adenylate-cyclase-activating polypeptide (*pacap*), a known antimicrobial, was especially enriched in a neuronal cluster. We confirm that PACAP is antiviral *in vitro* and that PACAP expression increases in the OB 1 day post-viral treatment. Our work reveals how encounters with viruses in the olfactory periphery shape the vertebrate brain by inducing antimicrobial programs in neurons and by altering host behavior.

Keywords: olfactory bulb, zebrafish, virus, neuronal activation, neuropeptides, antiviral

Introduction

The nervous and immune systems work in tandem to recognize, escape, and eliminate pathogens (Kraus et al., 2021). Even in basal metazoans like ctenophores and cnidaria, bidirectional neuroimmune communication in specialized sensory cells influences motility and immunity (Babonis et al., 2018; Klimovich et al., 2020; Kraus et al., 2021; Pita et al., 2018; Rivera et al., 2012; Varoqueaux et al., 2018). In vertebrates, pathogens can influence immune responses by directly activating sensory neurons (Chiu et al., 2013; Pinho-ribeiro et al., 2023; Sepahi et al.,

2019). In mammals, sensory neurons at mucosal barriers are heavily studied because of their close proximity to pathogens, their ability to transmit pathogen signals from the periphery to the brain, and their potent immune regulatory functions. As such, sensory neurons found at mammalian mucosal barriers are the target of therapeutic interventions from pain and itch to infectious diseases (Chesné et al., 2019; Godinho-Silva et al., 2019; Huh and Veiga-Fernandes, 2020; Pinho-Ribeiro et al., 2017).

Chemosensing olfactory sensory neurons (OSNs) in the nasal mucosa directly contact the environment, relay information to the brain, and shape animal behavior from feeding to mating and predator avoidance (Curtis, 2014; Padilla-Coreano et al., 2019, 2016). Exposure to the environment leaves OSNs, and the olfactory bulb (OB) they project to, vulnerable to viral infection (Mori et al., 2002; Moseman et al., 2020; Van Riel et al., 2015; Wheeler et al., 2017). Despite this exposed localization, viral infection of the CNS via the olfactory route is rare (Butowt et al., 2021). This is because OSNs and other cells in the nasal mucosa coordinate rapid and effective antiviral immune responses to staunch viral spread (Ai and Klein, 2020; Bi et al., 1995; Durrant et al., 2016; Kurhade et al., 2016; van den Pol et al., 2014). In support, disruption of the olfactory epithelium and destruction of OSNs results in impaired antiviral immunity in the OB, indicating that neurons play an important role in protection of the CNS (van den Pol et al., 2014).

Neuroimmune interactions of the olfactory axis are often studied during active infection of neurons. In the OB, neurons can directly detect vesicular stomatitis virus (VSV) via pattern recognition receptors and secrete chemokines to recruit immune cells necessary for viral clearance (Ghita et al., 2021). Furthermore, microglia in the OB act as antigen presenting cells to T cells in the VSV infection model (Moseman et al., 2020). Overall, the OB has been proposed

to be an immuno-sensory region of the CNS based on evidence from mouse models where viruses actively infect the OB (Durrant et al., 2016).

Neuropeptides are small chemical messengers released by neurons. Beyond their well-known neurotransmitter functions, neuropeptides link innate immunity and the nervous system via potent antimicrobial functions (Brogden et al., 2005). Antimicrobial activity in neuropeptides is an ancestral feature of the metazoan tree of life as illustrated by the diversity of *Hydra* neuropeptides which shape the microbiome via their antibacterial properties (Augustin et al., 2017; Klimovich et al., 2020). Other examples of neuropeptides with known antimicrobial activities include substance P, neuropeptide Y (NPY) or pituitary adelylate cyclase activating polypeptide (also known as PACAP) (reviewed by Brodgen et al., 2005). In both invertebrates and vertebrates, the olfactory system expresses several neuropeptides including NPY and PACAP (Hansel et al., 2001; Hussain et al., 2016). Neuropeptide functions in olfactory circuits include neuromodulation, regulation of neurogenesis, learning and behavior (Chalasani et al., 2010; Hansel et al., 2001; Hussain et al., 2016; Lindsay et al., 2022; Salesse et al., 2012). However, how pathogens reaching the olfactory system impact neuropeptide expression and whether this is a mechanism for pathogen control is currently unknown.

Neurons can transmit the presence of a pathogen within milliseconds and rapidly release soluble mediators thereby increasing velocity of immune responses (Cohen et al., 2019; Friedrich and Laurent, 2004). We previously reported that the presence of a live virus, infectious hematopoietic necrosis virus (IHNV), in the olfactory organ of teleost can generate neuronal signals and very rapidly induce expression of select immune transcripts in brain tissues (Larragoite et al., 2016; Sepahi et al., 2019). However, whether these ultra-fast immune responses impact neuronal states in the brain, specifically in the OB, and whether they are integrated into behavioral responses is

unknown. Here we present a zebrafish model to investigate the neuroimmune interactions that occur in the OB of zebrafish in response to presence of a virus in the periphery.

Results

In rainbow trout, intranasal (I.N.) delivery of IHNV causes apoptosis in a subset of OSNs in the olfactory organ (OO) as rapidly as 15 minutes (m) as the lymphocyte cellular landscape and chemokine expression profile changes in the OB (Sepahi et al., 2019). While live attenuated IHNV is present in the olfactory organ of rainbow trout until 4 days (d) post I.N. delivery, viral RNA is never detected in the brain (Larragoite et al., 2016). Here we adapted this model to adult zebrafish. Virulent IHNV has been used to infect zebrafish before by adapting the virus to the warmer host temperatures (Aggad et al., 2010; Levraud et al., 2014; Ludwig et al., 2011). However, we aimed to restrict the presence of the virus to the olfactory organ and avoid penetration of the brain. Using I.N. delivery of live attenuated IHNV at the normal host temperature (28□), we measured the phenotype changes in the OB and the kinetics of the viral detection in the OO and OB (Figure 1). By qPCR we only detected RNA of the IHNV nucleoprotein 15 m after I.N. delivery, and it was never detected in the OB (Figure 1B). This confirmed that in our model IHNV is only transiently present in the olfactory periphery and does not reach the OB.

Detection of live attenuated IHNV triggers behavioral changes in adult and larval zebrafish

We wanted to determine if zebrafish respond behaviorally to live virus. First, we tested adult animals I.N. treated with IHNV or vehicle controls and monitored swimming behavior in an open field paradigm 15 m or 1 d post-treatment (Baker et al., 2018). We observed significant

behavioral changes in adult animals at 1 d, but not 15 m. Specifically, treated zebrafish had decreased mean velocity, potentially indicative of classical sickness behavior (Figure 1C-D).

We also investigated if 6 day post-fertilization (dpf) larvae also exhibit behavioral changes to live viral detection. In this model, larvae were exposed to the virus or a vehicle in the water for 30 seconds and swimming behavior was tracked for 22 minutes. When exposed to IHNV, larva swam at significantly lower velocities, and displayed a trend towards increased turning behavior (Figure 2A-B) compared to the vehicle. Decreased velocity in larvae is a known stress response (Lopez-Luna et al., 2017). Together, our results indicate that olfactory detection of IHNV by both adult and larval zebrafish is integrated in higher areas of the brain and translates into behavioral responses.

Viral-specific activation of neurons in the OO and OB of larval zebrafish

In the rainbow trout live attenuated IHNV causes action potentials in the OSNs, as measured by EOG (Sepahi et al., 2019), but electrical responses in the teleost brain were not recorded. Because I.N. IHNV caused behavioral changes in adult and larval zebrafish, we asked whether live attenuated IHNV could activate OSNs and consequently neurons within the OB. We live imaged Tg(elavl3:GCaMP6S) 5 dpf larva by two-photon microscopy and recorded calcium-dependent fluorescent signals. Results show the presence of regions of interest (ROIs) in the OB which are specifically activated by IHNV but not KCl (positive control) or culture medium + 5% FBS (vehicle control for IHNV) (Figure 2C-E). As expected, there were ROIs only activated by KCl and these ROIs have a widespread localization in the OB (Figure S1). Therefore, larval zebrafish reveal the OB is activated by transient interactions with IHNV in the OO concordant with behavioral changes.

scRNA-Seq of the zebrafish OB after intranasal IHNV reveals changes to the cellular landscape

Given observed neuronal activation of the OB and behavioral changes, we sought to identify potential molecular changes in the OB at the single cell level following I.N. IHNV delivery. While scRNA-Seq has been performed on the OB in a murine model of olfactory occlusion (Tepe et al., 2018), comprehensive single cell transcriptomic studies have not been performed in the zebrafish OB. We identified a total of 4 lymphocyte clusters, 8 microglia clusters, 5 neuronal clusters, and 2 oligodendrocyte clusters integrating vehicle and IHNV treated datasets (Figure 3A-B).

Microglia1, Microglia2 and Microglia4 constitute the majority of microglia sequenced (Figure S2) and express classical microglial markers (*apoeb, mpeg1.1,* and *marco*) in addition to markers for mobile, ameboid and phagocytic microglial phenotype (*ccl34b.1* and *cd63*) (Figure S2&S4) (Mathys et al., 2017; Silva et al., 2021; Wu et al., 2020). At 15 m post I.N. IHNV treatment, Microglia1 and Microglia2 proportions both significantly expand relative to the 15 m I.N. controls (Figure 3C-D & S3A-C) suggesting a quick increase in activated microglia following I.N. IHNV delivery. Gene ontology (GO) of differentially regulated genes from these rapidly expanding microglial clusters at 15 m after virus compared to vehicle treated microglia shows enrichment of positive regulation of nervous system development and response to hypoxia. Hypoxia response was particularly interesting as it has been related to antiviral defense (Huang et al., 2021) (Figure S4).

Microglia3 express many of the same markers as Microglia1-2 but have higher expression levels of MHC II features such as *cd74a* and *cd74b* suggesting they are professional antigen presenting

cells (APCs) (Figure S2&S4). Microglia3 and 5 also express a separate subset of known zebrafish microglial markers but may represent infiltrating macrophage phenotypes since they express *ccl19a.1* and *siglec15l* (Figure S2&S4) (Oosterhof et al., 2018). These clusters also express anti-inflammatory *tnf-b* and *grn2* (Figure S4). Further, Microglia4 and Microglia8 express *il4* and *il13*, characteristic of a type II, anti-inflammatory state (Quarta et al., 2020). Conversely, Microglia6 express pro-inflammatory markers (*mmp2* and *mmp14*) (Figure S2) (Könnecke and Bechmann, 2013). At 1 d after I.N. IHNV treatment, changes in microglia clusters were less profound than at 15 m. At 1 d, *mmp2* expressing Microglia6 is expanded (Figure 3C-D & S3A-C). This is particularly interesting as *mmp2* has been shown to affect function of neuronal progenitors *in vitro* (Li et al., 2017). Lastly, Microglia8 is a small cluster characterized by expression of thus far unannotated genes (Figure S2). Combined, these data show that OB microglia mount rapid and complex immune responses to peripheral viruses in zebrafish.

We previously reported that $CD8^+$ T cells migrate into the OO of rainbow trout 15 m after I.N. IHNV concurrent with an egress of $CD8^+$ T cells from the OB (Sepahi et al., 2019). Moreover, we found that the cellular landscape of lymphocytes changes after I.N. SARS-CoV-2 S RBD in the zebrafish OO (Kraus et al., 2022). These findings made us look for lymphocyte clusters and their responses in the zebrafish OB scRNA-Seq dataset (Figure S5). One caveat to this data set is that animals were not perfused and therefore lymphocytes residing in the OB vasculature were likely included in the OB single cell suspensions. Further, the medium used during extraction was optimized for neuronal survival rather than viability of immune cells and consequently the lymphocyte clusters did not have high sequencing depth. Despite these caveats we captured 4 lymphocyte clusters.

In the vehicle treated OB, approximately 20% of collected cells clustered as Lymphocyte1 and 15% of cells clustered as Lymphocyte2 (Figure S5A). Further, approximately 5% of cells were B cells clustered in Lymphocyte3 (Figure S5A). Lymphocyte1 cells expressed many markers associated with NK cells in zebrafish (*ccl38.6, ccl34b.4,* and *ccl38a.5*) as well as multiple novel immune type receptors (*nitr*) thought to function as natural killer (NK) cell receptors and are therefore an innate-like cluster (Figure S2) (Carmona et al., 2017; Wei et al., 2007). Lymphocyte2 cells express classical markers of T cells including *cd4, cd8,* and *cxcr4* (Figure S2). Interestingly, 1 d after I.N. IHNV, a fourth cluster of lymphocytes emerged (Figure S3). Lymphocyte4 expresses *cd4* as well as *foxp3a,* the master transcription factor and marker for T_{regs} (Morikawa and Sakaguchi, 2014 (Figure S2)). While the lymphocyte populations do not change within timepoints, at 1 d Lymphocyte2 (classical T cell cluster) becomes the dominant cluster rather than innate-like cluster Lymphocyte1 which is the larger lymphocyte cluster in the integrated 15 m samples (Figure S3).

Re-clustering cells from Lymphocyte1, Lymphocyte2, and Lymphocyte4 with 5 significant principal components (PCs), reveals 6 distinct populations of non-B cell lymphocyte clusters (Figure S5). While all clusters express potential zebrafish NK markers (*ccl38.6* and *ccl34b.4*) and to a lesser extent *nitrs,* there are some differences across clusters (Figure 3C). For example, only two clusters express apoptosis-inducing serine kinase *gzm3.4,* indicating they are cytotoxic. Interestingly, neither of these clusters express *cd8a* or *cd8b,* and one of them expresses *rorc,* the gene for transcription factor Ror-gt, indicating that these clusters are likely cytotoxic NK cells (red) and ILC3 (mint green) (Figure S5C). One cluster (purple) expressed *il4* and *il13* and therefore may be ILC2s (Figure S5C). Importantly, there is one cluster (grass green) that

expresses both *cd4* and *foxp3a* indicating that they are T_{reg} cells. Overall, these ILC-like expression profiles like those of zebrafish gut ILCs (Hernández et al., 2018).

Within the neuronal clusters, neuron2 and neuron3 appear to be mature neurons expressing markers such as *pcdh7a, pcdh17,* and *olfm1b* (Figure S2) (Kanageswaran et al., 2015). Neuron3 are likely granule cells based on their expression of glutamate receptors (*grm1a* and *grm2a*) and GABA transport components (*slc32a1*) (Nagayama et al., 2014) (Figure S2). Overall, previous NGS endeavors have uncovered few genetic markers for mitral cells in mice, and almost none of these were found within our zebrafish mature neuron clusters (Tepe et al., 2018; Zeppilli et al., 2021). Classical mitral cell markers *cdhr1a* and *tbx21* were not detected in our data set, but we hypothesize that Neuron2 represent mature mitral cells based on glutamate associated genes present (*gad* and *gad1b*) (Böhm et al., 2020; Nagayama et al., 2014; Zeppilli et al., 2021 (Figure S2)).

Neuron1 is an interesting cluster expressing immune related features (*ifn-g* and *ptgdsb.1*) in addition to an aquaporin gene (*aqp1a.1*) that has been linked to adult neurogenesis (Figure S2) (Zheng et al., 2010). Interestingly, IFNg is expressed in axonimized motor neurons and is important in differentiation and neurogenesis in the murine adult subventricular zone (Olsson et al., 1989; Pereira et al., 2015). Further, Neuron1 cells express many factors associated with neuronal neurogenesis (*nog2*, *mdka*, *notch3*, *sox2* and *her6*) and are likely progenitors recently migrated from the subventricular zone (Figure S2) (Lübke et al., 2022; März et al., 2010; Peretto et al., 2004; Rieskamp et al., 2018; Schmidt et al., 2013). While Neuron4 and Neuron5 clusters express markers of progenitor neurons, they also have markers that suggest they are further along in differentiation programs such as *Lhx9*, *neurod1* and *gap43* (Figure S2) (Schmidt et al., 2013). Neuron5 was only found in the 1 d IHNV data set, indicating an increase in the proportion of

differentiating neurons that have gained a unique phenotype from viral exposure (Figure S3). After 1 d I.N. IHNV Neuron1 and Neuron5 have increased in proportion relative to the control cell suspensions (Figure 3C-D & S3A-C). There were 2 clusters of oligodendrocytes each expressing marker (*olig2, olig1,* and *sox10*) (Figure S2) (Takada et al., 2010; Tepe et al., 2018).

Transcriptional profiles of OB neurons reveal increased developmental program at 1 d after intranasal delivery of virus

1 d after I.N. IHNV we observed many differentially regulated features pertaining to neurogenesis and differentiation. In mature Neuron3 *ucp2* is significantly upregulated, and cells in progenitor like clusters Neuron1 and Neuron5 also express more *ucp2* (Figure 4A-C). Murine studies showed *ucp2* to be necessary for normal proliferation and differentiation in embryonic neurogenesis (Ji et al., 2017) and UCP2 is an important regulator of innate immune responses via mROS inhibition (West et al., 2011). Neuron2 has upregulated *nrn1a,* known to facilitate neurite growth, and *irs2b,* important for neuronal proliferation during brain development and involved intracellular insulin signaling (Schubert et al., 2003; Shimada et al., 2016, 2013) (Figure 4A-C). Neuron5 significantly downregulates *tac1,* which can be alternatively spliced into substance P and neurokinin A and is known to be expressed in the zebrafish olfactory system and inhibit olfactory stimulus in glomeruli across the animal kingdom (Nässel et al., 2019; Ogawa et al., 2012) suggesting a release of repressive signals (Figure 4A-C, E). Further, Neuron5 has significantly up-regulated *her15.2* and *pax6* which have both been associated with axonal growth in adult neurons (Figure 4A-B) (Mizoguchi et al., 2020; Sebastián-Serrano et al., 2012). Neuron1 and Neuron4 clusters have upregulated many transcription factors involved in differentiation (*nfia, zic2, sox6,* and *zfhx4*) and plasticity (*nfil3*) of neurons (Batista-Brito et al., 2009; Hemmi et al., 2006; Plachez et al., 2012; Tiveron et al., 2017; Van Der Kallen et al., 2015) (Figure 4A-C).

Gene ontology of differentially expressed genes across neuronal clusters 1 d after I.N. IHNV relative to controls show biological processes such as neuropeptide signaling, CNS and glial development, and cell differentiation are enriched after viral treatment (Figure 4D) (Zhou et al., 2019). Overall, this data indicate that zebrafish OB neuronal clusters are increasing expression of genes with predicted functions in neurogenesis 1 d after I.N. IHNV treatment relative to control treated neurons.

To understand our scRNA-Seq data we performed *in vivo* Edu labeling of proliferating cells which may explain the increases in immature neuronal populations in response to virus. No increase in proliferation in the OB 1 d after I.N. IHNV was found (Figure S6). Therefore, while there is an increase in progenitor-like neurons following I.N. IHNV treatment detected by scRNA-Seq, it is not due to proliferation within the OB.

The most highly enriched gene ontology pathway in neurons was the neuropeptide signaling pathway and highlighted genes such as *adcyap1b* (also known as *pacap*), *npb*, *penkb*, *scg5*, and *tac1* (Supplemental Table 1). Feature plots reveal that *pacap (adcyap1)*, an evolutionarily conserved neuropeptide (Cardoso et al., 2020), is specifically expressed in clusters Neuron 4 and Neuron 5, which are expanded 1 d after I.N. IHNV (Figure 4E&S3). *pacap* was very lowly expressed in microglia8 and was not found in any other immune clusters. Further, the PACAP specific receptor *adcyap1r11* (or *pac1*) was expressed in mature neuron clusters, while VIP receptors (*vipr1a*, *vipr1b*, and *vipr2*), which PACAP is also a ligand for, were not detected in our transcriptomes (Figure 4E). Because PACAP-38 has been shown to be antimicrobial in both teleost and mammals (Lee et al., 2021; Semple et al., 2019) and to regulate feeding behavior in fish (Lugo et al., 2010) but not implicated in antiviral immunity we decided to investigate this observation further.

PACAP immunoreactivity increases in the zebrafish OB 1 d after I.N. but not I.P. IHNV delivery

To confirm our scRNA-Seq results, we performed immunofluorescence staining using an antibody against PACAP-38, using a commercially available anti-mouse PACAP-38 antibody. We performed amino acid alignments of zebrafish and mouse PACAP and determined 89% identity between both sequences as previously described in other comparative studies (Figure S8). We compared zebrafish treated I.N. IHNV or vehicle 1 d following delivery because at this time point we observed changes in both behavior and transcriptional profiles of neurons. We found that PACAP-38 immunoreactivity is significantly higher in the OB of I.N IHNV treated zebrafish compared to those which received vehicle (Figure 5A-C). The isotype control showed no immunoreactivity (Figure S7). Since PACAP responses have been detected in the mouse brain in the context of systemic inflammation or infection (Lee et al., 2021), we compared PACAP responses in the OB of zebrafish I.P. injected with IHNV or vehicle at the same time point. In contrast with the I.N treatment, I.P. injected animals had decreased numbers of PACAP-38^{+} cells in the OB compared to vehicle controls (Figure 5D-F). These results confirm that olfactory detection of IHNV triggers a neuronal PACAP response in the zebrafish OB.

PACAP-38 has antiviral activity against IHNV in vitro

To determine if the onset of *pacap* expression by immature neurons in the OB represents an antiviral immune program in zebrafish, we tested PACAP antiviral activity *in vitro*. We used recombinant amidated and non-amidated forms of PACAP-38 from the teleost *Clarias gariepinus* which has a 92% amino acid identity with *D. rerio* PACAP (Figure S8) (Lugo et al.,

2008). Of note, amidated PACAP-38 is the natural, biologically functional form of PACAP found in vertebrates (Hansel et al., 2001). As an experimental control for recombinant protein cytotoxicity, we evaluated viability of teleost cell line Epithelioma papulosum cyprini (EPC), the standard method for propagating IHNV. Results from cell viability assays (Figure S9) show that the active amidated PACAP-38 was non-toxic at concentrations up to 100nM. At the lowest concentration of recombinant protein tested (10nM) for cytotoxicity, non-amidated PACAP-38 exhibited cellular toxicity with 85.6% EPC cell viability (Figure S9).

Next, we tested whether PACAP-38 (aminated and non-aminated) protects EPCs from cell death when infected with virulent IHNV. No antiviral effects were observed for the non-active form PACAP-38 at any concentration tested (Figure 6). The active form of amidated PACAP-38 provided protection from virulent IHNV infection in a dose-dependent manner (Figure 6). Up to 70% protection was achieved at the concentration of 1μM when the active PACAP-38 was added to the cells together with the virus during the infection period (competition assay) (Figure 6). EPC cells without PACAP-38 (either active or inactive) with IHNV showed typical morphologies of viral cytopathic effect (CPE). CPE was reduced at increasing concentrations of the active amidated PACAP-38 (Figure 6). Similar results were obtained in post-infection assays, where PACAP was added after the infection with IHNV (Figure 6).

Discussion

Chemosensory systems detect and respond to environmental dangers; the integration of these signals by the brain is essential for animal survival. The chemosensory olfactory system detects odorants and sends signals to higher regions of the brain via the OB. OSNs directly sense the environment and project their axons into the OB, making them perfect danger sensors (Van Riel

et al., 2015). Protecting the CNS from pathogen translocation falls to the OB, a dynamic region of the brain known to participate in immune defense (Bi et al., 1995; Christian et al., 1996; Durrant et al., 2016; Kalinke et al., 2011; Kurhade et al., 2016; Leyva-Grado et al., 2009). Immune responses in the OB have been described using murine models of neurotropic pathogen infection where pathogens could be detected in the OB following different routes of infection (Dinn, 1980; Flexner, 1936; Song et al., 2021; Torres-Fernández et al., 2018; Van Riel et al., 2015; Wheeler et al., 2017). For example, I.N. infection with vesicular stomatitis virus leads to short infection of the OB without spread to the CNS. This is achieved by expression of type I interferons across the brain, which is abrogated when the olfactory epithelium is chemically ablated (van den Pol et al., 2014). However, immune responses in the OB caused by pathogen detection or damage in the olfactory periphery without translocation into the brain are not well understood.

Microorganisms and their products can directly interact and be recognized by neurons (Baral et al., 2016; Chiu et al., 2013; Pinho-ribeiro et al., 2023). In teleost, IHNV directly interacts with TrkA expressed on a subset of OSNs and triggers electrical signals in the olfactory epithelium (Sepahi et al., 2019). Furthermore, teleost OB responds to the presence of virus in the peripheral OO without viral translocation by regulating innate immune gene transcription (Sepahi et al., 2019). It is unknown how rapidly neuroimmune responses in the OB prepare the brain for pathogen invasion. We present a new zebrafish model that provides a better understanding of how transient peripheral viral encounters in the peripheral OO trigger neuroimmune responses in the OB which are computed into behavioral change.

While some strains of IHNV can be neurotropic, in rainbow trout live-attenuated IHNV can only be detected in the OO up to 4 d after I.N. delivery and never enters the brain (La Patra et al.,

1995; Larragoite et al., 2016). In the present zebrafish model, live attenuated IHNV is only detectable in the OO of adult zebrafish 15 m after I.N. delivery and does not translocate to the OB. However, transient presence of a virus is enough to cause changes in behavior. Zebrafish are a powerful animal model in neuroscience in part due to behavioral features that can be used as a readout for human actions (Stewart et al., 2014). One such behavior is avoidance of infected conspecifics; a behavior evolutionarily conserved across metazoans (Curtis, 2014; Kraus et al., 2021). Zebrafish exposed to conspecific alarm substances, thought to be largely composed of skin-commensals released from damaged skin cells, display a fear response characterized by increased darting episodes and erratic behavior which can be learned (Mathuru et al., 2012; Maximino et al., 2018). Interestingly, when adult zebrafish are exposed to heat lysed commensals, there is limited darting response, although there is a fear response like alarm substance-evoked behavior (Chia et al., 2019). Responses to conspecific alarm substance and commensal bacteria are at least in part informed by the olfactory system as evidenced by calcium imaging (Chia et al., 2019; Mathuru et al., 2012). Here adult and larva had decreased swimming velocity 1 d after I.N. IHNV, indicating potential sickness behavior. In support, larva showed an anxiety-like response to virus by decreasing their speed (Lopez-Luna et al., 2017). Future studies looking at behavioral changes to a variety of nasal pathogens will seek to clarify fear responses and correlate them to neuronal activation states using transgenic, OSN-ablated lines. Further, behavioral changes following multiple olfactory encounters with the same virus is of great interest to us, particularly to understand whether “memory” to olfactory pathogen exposure impacts the brain not only immunologically but also cognitively.

While it is known that viruses can cause damage to the olfactory epithelium and OB in post-viral olfactory dysfunction, there is little information about the immediate responses of OSNs to

viruses. Our work has ascertained that OSNs can smell live attenuated IHNV and send action potentials to the OB, measured by EOG (Sepahi et al., 2019). Interestingly, when SARS-CoV-2 S RBD is delivered intranasally, EOG magnitudes in response to food and bile acid odorants decrease significantly (Kraus et al., 2022). While the latter study enforces zebrafish as a model for olfactory dysfunction, the discrepancies between both studies highlight the wide effects that viruses and their proteins can have on olfactory physiology. In the current study, we show through calcium imaging in zebrafish larvae that IHNV specifically activates neurons in the OB. We did not identify which OSN subsets become activated in response to IHNV, nor did we observe activation of specific glomeruli in the zebrafish OB. This suggests that multiple OSN types may be responsive to IHNV and motivates future experiments comparing different viruses. This is of particular interest because stimulation with specific odorants has been shown to influence which olfactory receptors neuronal progenitors will express as they mature; this may result in biased expression of olfactory receptors that would alert an organism to danger more rapidly after being around conspecifics shedding pathogen (van der Linden et al., 2020).

Our work shows that neuroimmune responses take place in the OB upon detection of viruses in the olfactory periphery. We provide single cell maps of complex, transient responses, which we hope are useful to many others in the field. One of the challenges of scRNA-Seq is assigning identities to cell clusters not previously characterized, particularly when working with non-mammalian model organisms. For instance, scRNA-Seq of the murine OB has not uncovered many definitive markers for mature OSNs, and few previously suggested markers were found in our zebrafish OB dataset (Tepe et al., 2018; Zeppilli et al., 2021). Therefore, while we captured 5 distinct clusters of neurons, 2 of which represent mature functional subsets and 3 are more progenitor-like by their transcriptional profiles, we cannot determine definitively if we captured

interneuron subsets. Our method for capturing single cell suspensions was optimized for neuronal survival, yet neurons only represent about a third of the cells in our dataset after quality control. Our results nevertheless show that detection of viruses in the periphery shapes neuronal transcriptional profiles and populations in the OB. Specifically, at 1 d after I.N. IHNV treatment, neuronal progenitor-like clusters had increased in proportion compared to controls and significantly upregulated expression of genes associated with neuronal differentiation. While acute damage activates quiescent basal stem cells in the olfactory epithelium, chronic damage leads to these horizontal basal cells to enter an inflammatory state (Chen et al., 2019, 2017). Unlike mammals, zebrafish are well known for the regenerative abilities of their adult neurons under inflammatory signaling (Kyritsis et al., 2012). Interestingly, damage to muscle cells can alert distant muscle stem cells into an alert state (Rodgers et al., 2014). In mice, neural stem cells that will migrate to the OB and become mature neurons show unique inflammatory profiles as they leave quiescence and can be activated by systemic TNF-α (Belenguer et al., 2021). Here, we present evidence that inflammation in the peripheral OO may prime the progenitor-like neuronal pool in the OB, perhaps as a mechanism to retain plasticity which may be needed if neuronal damage occurs. Further, PACAP is exclusively expressed in these progenitor-like clusters. Since PACAP is necessary for survival and differentiation of developing neurons, this is to be expected (Han and Lucero, 2006; Hegg et al., 2003; Irwin et al., 2015). However, there was no damage to our model because the virus did not reach the OB and therefore the increased populations of PACAP expressing progenitor-like neurons suggests an antiviral role for these cells. Indeed, we show that PACAP is antiviral in culture, tying neuronal differentiation processes and immune function. These results demonstrate the neuropeptides commonly

expressed in the olfactory system can act as neurotransmitters as well as innate immune mediators.

In summary, the present study reveals that virus-elicited olfactory neuronal signals are integrated and translated into behavioral responses in zebrafish. Peripheral viral detection impacts transcriptional programs in neurons, glia and immune cells in the OB creating altering neuronal differentiation programs. Immature neurons in the OB appear to be poised to participate in antiviral immunity via PACAP expression. Our work highlights the importance of investigating neuroimmune communication along the olfactory-brain axis and suggests that brain immunity and behavior are sculpted by chemosensory pathogen detection.

Materials and Methods

Zebrafish: Founders of our AB colony were obtained from ZIRC (Oregon, USA) and maintained at the University of New Mexico Castetter Hall Animal Research Care facility's zebrafish facility at 28°C and a 14-hour light and 10-hour dark cycle. Fish are maintained using a Gemma diet (Skretting). All animals used for this study were adults between 1-1.5 years of age. For the behavioral and single cell AB zebrafish were maintained in 6-L mixed sex tanks on the same custom-built recirculating system with solid filtration at 27°C and a 14-hour light and 10-hour dark cycle. For these studies sex was considered as a variable and data represents evenly both sexes. For larval studies, 5 days post fertilization GCamP6S zebrafish larvae were maintained on a *nacre* background at the Harvard Neuroscience Department Zebrafish Facility. For two photon imaging, larvae were mounted on a Petri dish containing a drop of 2% low melting agarose prepared in tank water. A window was carefully cut with a sterile scalpel blade to expose the olfactory pits of the animal to the surrounding water. A second window was

created from the pectoral fins to the tail so that the tail will be free moving. For larval behavioral studies, 5 dpf wild type zebrafish were used as described below. All procedures were done with approval from the University of New Mexico's Institutional Animal Care and Use Committee under protocol number 22-201239-MC or the University of Nebraska at Omaha protocol number 17-070-09-FC.

Intranasal treatments of zebrafish: For intranasal treatments animals are anesthetized with 0.04 mg/ml Tricaine (Syndel) in tank water for 1 minute and then transferred to an absorbent boat soaked with anesthesia solution for the duration of treatment. If endpoints were the next day, animals were moved to the system overnight. Live attenuated infectious hematopoietic necrosis virus (IHNV) was at $2x10^8$ plaque forming units (pfus) as previously described (Fryer et al., 1976; La Patra et al., 2004) and approximately 5µl per nare was delivered using a microloader pipette (Eppendorf, 930001007). Animals were then moved to a recovery tank and monitored until end point time. Sterile PBS (approximately 5µll per nare) without magnesium and chlorine was a control for the anesthesia and mechanical perturbation of intranasal treatments.

qPCR detection of virus and RT-qPCR for chemokine expression: Olfactory organs or olfactory bulbs from 3 individual animals were dissected out and separately pooled in 500µl of trizol (Cat 15596026), then snap frozen. Tissue was homogenized by adding two tungsten beads to thawed trizol and shaken at 30 Hz for 5 minutes. RNA was extracted following the Trizol protocol as previously described for this tissue (Kraus et al., 2022). RNA was quantified and standardized for cDNA synthesis using Superscript III first stand system (Thermofisher 18080051). qPCR was performed using SSOadvanced supermix (Biorad 1725270) at a T_M of

62°C. Primers for N protein of IHNV are F: 5'-GGTCGCCGAACTTCTGGAA-3' and R: 5'-GTAGGGCGCAGGTGAAGAGG-3'.

Live imaging of neuronal calcium signaling in zebrafish larvae: 5 days post-fertilization Tg(elavl3:GCaMP6S) zebrafish larvae on a Nacre$^{-/-}$ background were embedded in 2% low melting point agarose and covered with facility water. The area from the olfactory pits to the most rostral part of the animal was freed from agarose using a scalpel. The tail was also freed by removing agarose posterior to the swim bladder. Tail movement in response to KCl stimulation was indicative of healthy animals. 2-P imaging of the olfactory bulb and the forebrain was done as previously described using random 10 s pulses of odorants directed to the olfactory pits every 2 minutes (Herrera et al., 2021). Odorants were either live attenuated IHNV, DMEM medium + 10% FBS as a negative control, or KCl as a positive control for the duration of the experiment. Image acquisitions and data analyses of calcium signals were performed as described (Herrera et al., 2021).

Larval behavioral studies: All experiments took place between 10am and 6pm. 6 dpf larvae were placed in the setup 5 min before the experiment started. In a custom-built setup, the fish experienced a constant water flow (about 34 ml/min) in a 4 cm x 4 cm chamber. Water was constantly flowing in on one side of the chamber and pumped out at the opposite side of the chamber. Meshes on both ends of the chamber prevented the fish from getting into the pump if they stopped swimming. A custom written software controls the system that allows for automatic stimulation with any liquid, for example a virus diluted in water. Two arduino controlled valves are switched between a constant water flow and the e.g., virus that is added to the constant water stream. Every fish received three 10-second-long presentations of either the virus or a vehicle and in addition three 10-second-long presentations of water as a control for valve switching

related changes in behavior. The order of the presentation of virus and control was alternated between fish. The inter stimulus interval between the presentations was 150 seconds. The virus/vehicle was cleared from the chamber at 120 seconds post-delivery.

Preprocessing and filtering of data was performed as follows. Fish coordinates $\vec{x}(t)$ were smoothed using a Savitzky-Golay filter of ~1/3 second (10 frames). Velocity was calculated as $\vec{v}(t) = \frac{\vec{x}(t-1)-\vec{x}(t+1)}{2 \cdot dt}$, and the speed is given by the magnitude of the velocity $s(t) = |\vec{v}(t)|$. To remove spurious data points that are likely due to tracking errors, we excluded all data points with speed equal to zero and points where the time difference dt, between two consecutive tracked coordinates was larger than 0.04s, which indicated a temporary loss of the fish by the tracking software.

we estimated the strength of the water flow dragging the fish back (see 'experimental setup') by first finding all instances where the fish was facing in the direction of the upcoming water flow with heading angle θ between $90°$ and $-90°$ (swimming directedly towards the flow is defined as $0°$) yet was moving 'backwards' with the flow. We then averaged all the fish velocity components that were parallel to the flow direction $\vec{v}_{flow} = \langle \vec{v}_{||} \rangle$, where $\langle \dots \rangle$ represent average over all velocity measurements.

Finally, we calculated the corrected velocity vector of the fish, correcting for the fact that the fish is swimming against the constant water flow $\vec{v}(t)_{corrected} = \vec{v}(t) - \vec{v}_{flow}$, and accordingly we have $s(t)_{corrected} = |\vec{v}(t)_{corrected}|$. We note that this calculation assumes a homogenous flow across the arena and therefore is only a representation of the average flow experienced by the fish.

Adult behavioral studies: Behavioral assays were conducted as previously reported (Baker et al., 2018). In short, square plexiglass arenas with an inner width of 12 inches were filled with 4 L of system water and left to settle inside a white curtained area. Camera was mounted above, and focused. Fish were alternatively intranasally treated with media (DMEM+5% FBS, used to grow IHNV) or live attenuated IHNV. Animals were anesthetized in 0.04 mg/ml Tricaine (Syndel) for 1 minute, intranasally treated, then left in a recovery tank for 5 minutes. Then they were placed in the arena and allowed to settle for 30 seconds before video recording for 5 minutes. Arenas were washed between trials. No water was allowed to cause color discrepancies under the arenas. Analysis of behavior was performed with EthoVision software. Animals that traveled less than 10 cm were removed from analysis.

Single cell isolation and capture: After animals were euthanized, the olfactory bulbs were dissected out and immediately placed in individual tubes with Neurobasal medium (Gibco Cat# 21103049) supplemented with 0.04% BSA and 5% FBS. This supplemented media was used throughout cell isolation and capture. Olfactory bulbs were gently rocked for 45 minutes, then all (N = 6) samples for a single treatment were mashed through a 100mm cell strainer into 3ml of supplemented media. Cells were washed 2 times by spinning 400 x g for 8 minutes, carefully removing supernatant and resuspending in fresh medium. When cells were pipetted up and down 3 seconds were counted for plunger movements up and down. Rainin low bind tips were used throughout. Cells were then sorted for viability using propidium iodide. Cells were washed once and resuspended in 60 ml. 10ml cells were used for counting with a hemocytometer and 10,000 cells were loaded in 40ml to the 10x chromium cell capture machine after running through a 40µm Flowmi cell strainer (Bel-art catalog no. H13680-0040) to remove clumped cells.

Libraries were prepped and sequenced by University of Nebraska DNA Sequencing Core. Sequencing metrics can be found in Figure S3A.

Analysis of single cell RNA-Seq: Fastqs were generated and processed into count matrices using Cell Ranger v3.0 under default settings using a reference generated using the GRCz11 zebrafish genome. In R (v3.4.1) and Surat (v3.1.1), matrices were imported into a Seurat object for analysis. As quality control, cells with less than 200 or greater than 2500 features and greater than 5% of features belonging to the mitochondria were removed. Counts were then normalized using the 'LogNormalize' method and a scale factor of 10,000. Using FindVariableFeatures under the 'vst' method, 2000 variable genes were found. Treatments were then integrated using the CCA method and scaled using default settings (Butler et al., 2018). Dimensional reduction was done first with PCA analysis using 30 significant principal components determined using Jackstraw and Elbow plot analysis. Secondary dimensional reduction was done with tSNE. Clusters were found using 'FindNeighbors' and 'FindClusters' sequentially at a resolution of 0.5 and 30 significant PCs. Differential expression was done using 'FindMarkers' set to default between treatments within each cluster and significant features with Bonferroni adjusted p-values of less than 0.05 were then exported for gene ontology. Plots were made in R using a combination of Seurat and ggplot2 (v3.3.5) elements. Gene ontology was done using Metascape, which produced the biological process bar plots (Zhou et al., 2019).

Antiviral and cell viability assays: EPC cells were maintained at 15 □ in MEM (Corning) supplemented with 10% FBS. IHNV stocks were grown in EPC cells as previously described (Ma et al., 2019). The cytotoxicity of the tested extract was evaluated using MTT assay

(CyQUANT™ MTT Cell Viability Assay). EPC cells (10000 cells/well) were prepared in 96-well plates for 24h. Cells were exposed to concentrations of PACAP-85% or amidated PACAP-96% samples in quadruplicate (10µM, 1µM, 100nM, 10nM and MEM vehicle control), followed by 48h incubation at 15 °C. Cell viability was measured using the CyQUANT MTT cell viability assay (Thermo Fisher Scientific Cat #V13154) following the manufacturer's protocol.

Three different assays were applied to investigate the antiviral activity of PACAP with various concentrations: pretreatment, competition, and post-treatment. All assays were performed in quadruplicate. For amidated PACAP-96%, concentrations of 1µM, 800nM, 600nM, 400nM and 200nM were used; for PACAP-85%, 50µM, 40µM, 30µM, 20µM and 10µM were used.For all treatments, EPC cells (10^6 cells/well) were prepared in 24-well plates for 24h. All infections were performed at a Multiplicity of Infection of 0.05. In the pretreatment assay, cells were treated with PACAP-85% or amidated PACAP-96% for 2h, then washed before infection with IHNV for 1h. In the competition assay, PACAP-85% or amidated PACAP-96% and IHNV (10^5 pfu/ml) were mixed and incubated at 15 °C for 2h. Mixtures were added to the monolayers of EPC cells for 1h. In the post-infection treatment assay, the monolayers of EPC cells were incubated with IHNV for 1h, rinsed, then treated with PACAP-85% or amidated PACAP-96% for 2h. Cells were washed twice with MEM, then incubated in MEM with 2% FBS at 15 °C and observed with an inverted microscope. After 7 days incubation, cell viability was measured using the CyQUANT MTT cell viability assay (Thermo Fisher Scientific) following the manufacturer's protocol. Virus-infected EPC cells and non-treated cells served as infection control and blank control, respectively. The relative survival of cells was calculated as:

[(OD value of treatment group − OD_{570} value of infection control)/(OD_{570} value of blank control − OD_{570} value of infection control)] × 100.

Immunofluorescence staining: 30 µm cryosections were stained with a polyclonal anti-PACAP-38 antibody (Abcam, ab216627). In short, heads were fixed overnight in 4% methanol-free PFA at room temperature, followed by 5 days in 10% EDTA, pH 7.2. Samples were cryoprotected in 33% w/v Sucrose in ddH2O until saturation, followed by flash freezing in Tissue-Tek OCT Compound (Sakura Finetek USA, catalog no. 4583). Samples were processed into 30 µm sections with a Leica CM3050S (Leica, Wetzlar, Germany) onto Superfrost Plus Slides (VWR catalog no. 48311-703). OCT was removed from sections displaying the olfactory bulb by 3 rinses for 5 minutes each in 1x PHEM, then permeabilized for 10 minutes with 0.5% Triton X-100 in 1x PHEM, followed by 2 rinses for 5 minutes each in 1x PHEM. Antigen retrieval was performed by covering samples in citrate buffer (0.1 M, pH 6.0) for 5 minutes at 90°C, followed by 3 rinses for 5 minutes each in 1x PHEM. Samples were blocked for 1 hours with BlockAid blocking solution (Thermo Fisher Scientific, catalog no. B10710)). Samples were incubated overnight at 4°C with anti-PACAP-38 antibody (Abcam, catalog no. ab216627, 1:100) or normal Rabbit IgG (Santa Cruz Biotechnology catalog no. sc-3888) in Pierce Immunostain Enhancer (Thermo Fisher Scientific catalog no. 46644) with 0.1% v/v Tween and 1% w/v Bovine Serum Albumin. Following incubation with primary antibodies, samples were rinsed twice for 5 minutes each in 1x PHEM. Samples were then incubated for 2 h with AlexaFluor 647 Goat anti-Rabbit (1:300, Jackson Immunoresearch catalog no. 111-605-144) diluted in 1x PHEM with 0.1% v/v Tween 20, 1% w/v Bovine Serum Albumin, 10% v/v Normal Donkey Serum, and 200 mg/ml DAPI. Samples were then rinsed three times for 10 minutes each, then mounted with Prolong Glass Antifade Mountant with NucBlue (Thermo Fisher Scientific catalog no. P36981). For each round of staining, an isotype control of normal Rabbit IgG was included. For Edu detection, zebrafish were injected intraperitoneally 1 day before sacrifice as previously described

(Lindsey et al., 2018) and detected following the click-it Plus for imaging protocol (Thermo Fisher Cat# C10640). Samples were imaged on a Zeiss LSM 780, equipped with an Xcite halogen lamp. All images for quantification to be compared with each other were imaged on identical settings. Images were captured as a .czi file, which was imported into Fiji using the Bioformats importer. Rois were placed around the center region of the olfactory bulb and mean gray value intensity measurements of each ROI were taken.

Statistical analysis: To check that data was normally distributed, an F test or Bartlett's test was done on all data. Parametric data with 2 groups for comparison were analyzed using a Student's T test or a Wilcoxon-signed rank test for comparison within groups. Population proportion analysis of cells in each cluster between clusters was analyzed using 'prop.test' and p-values were adjusted using 'p.adjust' set to 'bonferroni' method. All analyses were done in prism (v 9.3.1). For larval behavioral studies, statistics were performed as previously described (Herrera et al., 2021). IHNV and KCl-selective rois were identified by selecting rois with activity during the 30s following the onset of the chosen stimulus that was 1.6 times greater than the sum of the activities during the other two stimuli over the same time period.

Data availability: NCBI Bioproject Number is PRJNA839769.

Acknowledgements:

This work was partly funded by the ADVANCE UNM Women in Science Award to IS and the National Science Foundation award # 1755348. AK received support from the UNM Center for Advanced Research Computing (CARC). The authors would like to thank The University of Nebraska DNA Sequencing Core receives partial support from the National Institute for General Medical Science (NIGMS) INBRE - P20GM103427-14 and COBRE - 1P30GM110768-01 grants as well as The Fred & Pamela Buffett Cancer Center Support Grant - P30CA036727. We thank Drs. Yamila Carpio, Mario Pablo Estrada and Brian Dixon for sharing the recombinant PACAP-38. We thank Dr. Michael Paffett and the New Mexico Comprehensive Cancer Center's Fluorescence Microscopy and Cell Imaging core for technical and Drs. Lijing Bu and Marijan Posavi for bioinformatics support. This publication's contents are the sole responsibility of the authors and do not necessarily represent the official views of the NIH or NIGMS.

References:

Aggad D, Stein C, Sieger D, Mazel M, Boudinot P, Herbomel P, Levraud J-P, Lutfalla G, Leptin M. 2010. Signaling in Zebrafish 2 γ 1 and Ifn- γ In Vivo Analysis of Ifn- In Vivo Analysis of Ifn-g1 and Ifn-g2 Signaling in Zebrafish. *J Immunol* **185**:6774–6782. doi:10.4049/jimmunol.1000549

Ai S, Klein RS. 2020. Update on T cells in the virally infected brain□: friends and foes. *Neurology* **33**:405–412. doi:10.1097/WCO.0000000000000825

Augustin R, Schröder K, Murillo Rincón AP, Fraune S, Anton-Erxleben F, Herbst E-M, Wittlieb J, Schwentner M, Grötzinger J, Wassenaar TM, Bosch TCG. 2017. A secreted antibacterial neuropeptide shapes the microbiome of Hydra. *Nat Commun* **8**. doi:10.1038/s41467-017-00625-1

Babonis LS, DeBiasse MB, Francis WR, Christianson LM, Moss AG, Haddock SHD, Martindale

MQ, Ryan JF. 2018. Integrating embryonic development and evolutionary history to characterize tentacle-specific cell types in a ctenophore. *Mol Biol Evol* **35**:2940–2956. doi:10.1093/molbev/msy171

Baker MR, Goodman AC, Santo JB, Wong RY. 2018. Repeatability and reliability of exploratory behavior in proactive and reactive zebrafish, Danio rerio. *Sci Rep* **8**:12114. doi:10.1038/s41598-018-30630-3

Baral P, Mills K, Pinho-ribeiro FA, Chiu IM. 2016. Forum Pain and Itch: Beneficial or Harmful to Antimicrobial Defense? *Cell Host Microbe* **19**:755–759. doi:10.1016/j.chom.2016.05.010

Batista-Brito R, Rossignol E, Hjerling-Leffler J, Denaxa M, Wegner M, Lefebvre V, Pachnis V, Fishell G. 2009. The Cell-Intrinsic Requirement of Sox6 for Cortical Interneuron Development. *Neuron* **63**:466–481. doi:10.1016/j.neuron.2009.08.005

Belenguer G, Duart-Abadia P, Jordán-Pla A, Domingo-Muelas A, Blasco-Chamarro L, Ferrón SR, Morante-Redolat JM, Fariñas I. 2021. Adult Neural Stem Cells Are Alerted by Systemic Inflammation through TNF-α Receptor Signaling. *Cell Stem Cell* **28**:285–299. doi:10.1016/j.stem.2020.10.016

Bi Z, Barna M, Komatsu T, Reiss CS. 1995. Vesicular stomatitis virus infection of the central nervous system activates both innate and acquired immunity. *J Virol* **69**:6466–6472. doi:10.1128/jvi.69.10.6466-6472.1995

Böhm E, Brunert D, Rothermel M. 2020. Input dependent modulation of olfactory bulb activity by HDB GABAergic projections. *Sci Rep* **10**:1–15. doi:10.1038/s41598-020-67276-z

Brogden KA, Guthmiller JM, Salzet M, Zasloff M. 2005. The nervous system and innate immunity: the neuropeptide connection. *Nat Immunol* **6**:558–564. doi:10.1038/ni1209

Butler A, Hoffman P, Smibert P, Papalexi E, Satija R. 2018. Integrating single-cell

transcriptomic data across different conditions, technologies, and species. *Nat Biotechnol* **36**:411–420. doi:10.1038/nbt.4096

Butowt R, Meunier N, Bryche B, Bartheld CS Von. 2021. The olfactory nerve is not a likely route to brain infection in COVID 19: a critical review of data from humans and animal models. *Acta Neuropathol* **141**:809–822. doi:10.1007/s00401-021-02314-2

Cardoso JCR, Garcia MG, Power DM. 2020. Tracing the Origins of the Pituitary Adenylate-Cyclase Activating Polypeptide (PACAP). *Front Neurosci* **14**:366. doi:10.3389/fnins.2020.00366

Carmona SJ, Teichmann SA, Ferreira L, MacAulay IC, Stubbington MJT, Cvejic A, Gfeller D. 2017. Single-cell transcriptome analysis of fish immune cells provides insight into the evolution of vertebrate immune cell types. *Genome Res* **27**:451–461. doi:10.1101/gr.207704.116

Chalasani SH, Kato S, Albrecht DR, Nakagawa T, Abbott LF, Bargmann CI. 2010. Neuropeptide feedback modifies odor-evoked dynamics in Caenorhabditis elegans olfactory neurons. *Nat Neurosci* **13**:615–621. doi:10.1038/nn.2526

Chen M, Reed RR, Lane AP. 2019. Chronic Inflammation Directs an Olfactory Stem Cell Functional Switch from Neuroregeneration to Immune Defense. *Cell Stem Cell* **25**:501-513.e5. doi:10.1016/j.stem.2019.08.011

Chen M, Reed RR, Lane AP. 2017. Acute inflammation regulates neuroregeneration through the NF-κB pathway in olfactory epithelium. *Proc Natl Acad Sci* **114**:8089–8094. doi:10.1073/pnas.1620664114

Chesné J, Cardoso V, Veiga-Fernandes H. 2019. Neuro-immune regulation of mucosal physiology. *Mucosal Immunol* **12**:10–20. doi:10.1038/s41385-018-0063-y

Chia JSM, Wall ES, Wee CL, Rowland TAJ, Cheng RK, Cheow K, Guillemin K, Jesuthasan S. 2019. Bacteria evoke alarm behaviour in zebrafish. *Nat Commun* **10**:3831. doi:10.1038/s41467-019-11608-9

Chiu IM, Heesters BA, Ghasemlou N, Von Hehn CA, Zhao F, Tran J, Wainger B, Strominger A, Muralidharan S, Horswill AR, Wardenburg JB, Hwang SW, Carroll MC, Woolf CJ. 2013. Bacteria activate sensory neurons that modulate pain and inflammation. *Nature* **501**:52–57. doi:10.1038/nature12479

Christian AY, Barna M, Bi Z, Reiss CS. 1996. Host immune response to vesicular stomatitis virus infection of the central nervous system in C57BL/6 mice. *Viral Immunol* **9**:195–205. doi:10.1089/vim.1996.9.195

Cohen JA, Edwards TN, Liu AW, Hirai T, Jones MR, Wu J, Li Y, Zhang S, Ho J, Davis BM, Albers KM, Kaplan DH. 2019. Cutaneous TRPV1+ Neurons Trigger Protective Innate Type 17 Anticipatory Immunity. *Cell* **178**:919–932. doi:10.1016/j.cell.2019.06.022

Curtis VA. 2014. Infection-avoidance behaviour in humans and other animals. *Trends Immunol* **35**:457–464. doi:10.1016/j.it.2014.08.006

Dinn JJ. 1980. Transolfactory spread of virus in herpes simplex encephalitis. *Br Med J* **281**:1392. doi:10.1136/bmj.281.6252.1392

Durrant DM, Ghosh S, Klein RS. 2016. The Olfactory Bulb: An Immunosensory Effector Organ during Neurotropic Viral Infections. *ACS Chem Neurosci* **7**:464–469. doi:10.1021/acschemneuro.6b00043.The

Flexner BYS. 1936. Respiratory versus gastro-intestinal infection in poliomyelitis. *J Exp Med* **63**:209–26. doi:10.1084/jem.63.2.209.

Friedrich RW, Laurent G. 2004. Dynamics of Olfactory Bulb Input and Output Activity During

Odor Stimulation in Zebrafish. *J Neurophysiol* **91**:2658–2669. doi:10.1152/jn.01143.2003

Fryer JL, Rohovec JS, Tebbit GL, Mcmichael JS, Pilcher KS. 1976. Vaccination for control of infectious diseases in pacific salmon. *Fish Pathol* **10**:155–164. doi:10.3147/jsfp.10.155

Ghita L, Spanier J, Chhatbar C, Mulenge F, Pavlou A, Larsen P, Waltl I, Lueder Y, Kohls M, Jung K, Best SM, Förster R, Stangel M, Schreiner D, Kalinke U. 2021. MyD88 signaling by neurons induces chemokines that recruit protective leukocytes to the virus-infected CNS. *Sci Immunol* **6**:eabc9165. doi:10.1126/sciimmunol.abc9165

Godinho-Silva C, Cardoso F, Veiga-Fernandes H. 2019. Neuro-Immune Cell Units: A New Paradigm in Physiology. *Annu Rev Immunol* **37**:19–46. doi:10.1146/annurev-immunol-042718-041812

Han P, Lucero MT. 2006. Pituitary adenylate cyclase activating polypeptide reduces expression of Kv1.4 and Kv4.2 subunits underlying A-type K+ current in adult mouse olfactory neuroepithelia. *Neuroscience* **138**:411–419. doi:10.1016/j.neuroscience.2005.11.028

Hansel DE, Eipper BA, Ronnett G V. 2001. Regulation of Olfactory Neurogenesis by Amidated Neuropeptides. *J Neurosci Res* **66**:1–7.

Hegg CC, Au E, Roskams AJ, Lucero MT. 2003. PACAP is present in the olfactory system and evokes calcium transients in olfactory receptor neurons. *J Neurophysiol* **90**:2711–2719. doi:10.1152/jn.00288.2003

Hemmi K, Ma D, Miura Y, Kawaguchi M, Sasahara M, Hashimoto-Tamaoki T, Tamaoki T, Sakata N, Tsuchiya K. 2006. A homeodomain-zinc finger protein, ZFHX4, is expressed in neuronal differentiation manner and suppressed in muscle differentiation manner. *Biol Pharm Bull* **29**:1830–1835. doi:10.1248/bpb.29.1830

Hernández PP, Strzelecka PM, Athanasiadis EI, Hall D, Robalo AF, Collins CM, Boudinot P,

Levraud J-P, Cvejic A. 2018. Single-cell transcriptional analysis reveals ILC-like cells in zebrafish. *Sci Immunol* **3**:eaau5265. doi:10.1126/sciimmunol.aau5265

Herrera KJ, Panier T, Guggiana-Nilo D, Engert F. 2021. Larval Zebrafish Use Olfactory Detection of Sodium and Chloride to Avoid Salt Water. *Curr Biol* **31**:782-793.e3. doi:10.1016/j.cub.2020.11.051

Huang R, Huestis M, Gan ES, Ooi EE, Ohh M. 2021. Hypoxia and viral infectious diseases. *JCI insight* **6**. doi:10.1172/jci.insight.147190

Huh JR, Veiga-Fernandes H. 2020. Neuroimmune circuits in inter-organ communication. *Nat Rev Immunol* **20**:217–228. doi:10.1038/s41577-019-0247-z

Hussain A, Üçpunar HK, Zhang M, Loschek LF, Grunwald IC. 2016. Neuropeptides Modulate Female Chemosensory Processing upon Mating in Drosophila. *PLoS Biol* **14**:e1002455. doi:10.1371/journal.pbio.1002455

Irwin M, Greig A, Tvrdik P, Lucero MT. 2015. PACAP modulation of calcium ion activity in developing granule cells of the neonatal mouse olfactory bulb. *J Neurophysiol* **113**:1234–1248. doi:10.1152/jn.00594.2014

Ji F, Shen I, Zou W, Jiao J. 2017. UCP2 Regulates Embryonic Neurogenesis via ROS-Mediated Yap Alternation in the Developing Neocortex. *Stem Cells* **35**:1479–1492. doi:10.1002/stem.2605

Kalinke U, Bechmann I, Detje CN. 2011. Host strategies against virus entry via the olfactory system. *Virulence* **2**:367–370. doi:10.4161/viru.2.4.16138

Kanageswaran N, Demond M, Nagel M, Schreiner BSP, Baumgart S, Scholz P, Altmüller J, Becker C, Doerner JF, Conrad H, Oberland S, Wetzel CH, Neuhaus EM, Hatt H, Gisselmann G. 2015. Deep Sequencing of the Murine Olfactory Receptor Neuron

Transcriptome. *PLoS One* **10**:47. doi:10.1371/journal.pone.0113170

Klimovich A, Giacomello S, Björklund Å, Faure L, Kaucka M, Giez C, Murillo-Rincon AP, Matt AS, Willoweit-Ohl D, Crupi G, de Anda J, Wong GCL, D'Amato M, Adameyko I, Bosch TCG. 2020. Prototypical pacemaker neurons interact with the resident microbiota. *Proc Natl Acad Sci U S A* **117**:17854–17863. doi:10.1073/pnas.1920469117

Könnecke H, Bechmann I. 2013. The role of microglia and matrix metalloproteinases involvement in neuroinflammation and gliomas. *Clin Dev Immunol* **2013**:914104. doi:10.1155/2013/914104

Kraus A, Buckley KM, Salinas I. 2021. Sensing the world and its dangers□: An evolutionary perspective in neuroimmunology. *Elife* 10:e66706. doi:doi.org/10.7554/eLife.66706

Kraus A, Huertas M, Ellis L, Boudinot P, Levraud JP, Salinas I. 2022. Intranasal delivery of SARS-CoV-2 spike protein is sufficient to cause olfactory damage, inflammation and olfactory dysfunction in zebrafish. *Brain Behav Immun* **102**:341–359. doi:10.1016/j.bbi.2022.03.006

Kurhade C, Zegenhagen L, Weber E, Nair S, Michaelsen-Preusse K, Spanier J, Gekara NO, Kröger A, Överby AK. 2016. Type I Interferon response in olfactory bulb, the site of tick-borne flavivirus accumulation, is primarily regulated by IPS-1. *J Neuroinflammation* **13**:22. doi:10.1186/s12974-016-0487-9

Kyritsis N, Kizil C, Zocher S, Kroehne V, Kaslin J, Freudenreich D, Iltzsche A, Brand M. 2012. Acute inflammation initiates the regenerative response in the adult zebrafish brain. *Science (80-)* **338**:1353–6. doi:10.1126/science.1228773

La Patra S, Clouthier S, Anderson E. 2004. Current Trends in Immunotherapy and Vaccine Development for Viral Disease of Fish In: Leung K, editor. Current Trends in Th Estudy of

Bacteria Viral Fish and Shrimp Diseases. Singapore: World Scientific Publishing Co. Pte. Ltd. pp. 363–389.

La Patra S, Lauda K, Jones G, Walker S, Shewmaker B. 1995. Characterization of IHNV isolates associated with neurotropism. *Vet Res BioMed Cent* **26**:433–437.

Larragoite ET, Tacchi L, Lapatra S, Salinas I. 2016. An attenuated virus vaccine appears safe to the central nervous system of rainbow trout (Oncorhynchus mykiss) after intranasal delivery. *Fish Shellfish Immunol* **67**:223–230. doi:10.1038/ja.2013.113.Venturicidin

Lee EY, Chan LC, Wang H, Lieng J, Hung M, Srinivasan Y, Wang J, Waschek JA, Ferguson AL, Lee KF, Yount NY, Yeaman MR, Wong GCL. 2021. PACAP is a pathogen-inducible resident antimicrobial neuropeptide affording rapid and contextual molecular host defense of the brain. *Proc Natl Acad Sci U S A* **118**:e1817623117. doi:10.1073/PNAS.1917623117

Levraud J-P, Palha N, Langevin C, Boudinot P. 2014. Through the looking glass: witnessing host–virus interplay in zebrafish. *Trends Microbiol* **22**:490–497. doi:10.1016/j.tim.2014.04.014

Leyva-Grado VH, Churchill L, Wu M, Williams TJ, Taishi P, Majde JA, Krueger JM. 2009. Influenza virus- and cytokine-immunoreactive cells in the murine olfactory and central autonomic nervous systems before and after illness onset. *J Neuroimmunol* **211**:73–83. doi:10.1016/j.jneuroim.2009.03.016

Li Q, Michaud M, Shankar R, Canosa S, Schwartz M, Madri JA. 2017. MMP-2: A modulator of neuronal precursor activity and cognitive and motor behaviors. *Behav Brain Res* **333**:74–82. doi:10.1016/j.bbr.2017.06.041

Lindsay JH, Mathiesa LD, Daviesa AG, Bettingera JC. 2022. A neuropeptide signal confers ethanol state dependency during olfactory learning in Caenorhabditis elegans. *Proc Natl*

Acad Sci **119**:e2210462119. doi:10.1073/pnas.2210462119/-/DCSupplemental.Published

Lopez-Luna J, Al-Jubouri Q, Al-Nuaimy W, Sneddon LU. 2017. Impact of stress, fear and anxiety on the nociceptive responses of larval zebrafish. *PLoS One* **12**:10.1371. doi:10.1371/journal.pone.0181010

Lübke L, Zhang G, Strähle U, Rastegar S. 2022. mdka Expression Is Associated with Quiescent Neural Stem Cells during Constitutive and Reactive Neurogenesis in the Adult Zebrafish Telencephalon. *Brain Sci* **12**:284. doi:10.3390/brainsci12020284

Ludwig M, Palha N, Torhy C, Rie Briolat V, Colucci-Guyon E, Bré Mont M, Herbomel P, Boudinot P, Levraud J-P. 2011. Whole-Body Analysis of a Viral Infection: Vascular Endothelium is a Primary Target of Infectious Hematopoietic Necrosis Virus in Zebrafish Larvae. *PLoS Pathog* **7**:e1001269. doi:10.1371/journal.ppat.1001269

Lugo JM, Oliva A, Morales A, Reyes O, Garay HE, Herrera F, Cabrales A, Pérez E, Estrada MP. 2010. The biological role of pituitary adenylate cyclase-activating polypeptide (PACAP) in growth and feeding behavior in juvenile fish. *J Pept Sci an Off Publ Eur Pept Soc* **16**:633–643. doi:10.1002/psc.1275

Lugo JM, Rodriguez A, Helguera Y, Morales R, Gonzalez O, Acosta J, Besada V, Sanchez A, Estrada MP. 2008. Recombinant novel pituitary adenylate cyclase-activating polypeptide from African catfish (Clarias gariepinus) authenticates its biological function as a growth-promoting factor in low vertebrates. *J ofEndocrinology* **197**:583–597. doi:10.1677/JOE-07-0555

März M, Chapouton P, Diotel N, Vaillant C, Hesl B, Takamiya M, Lam CS, Kah O, Bally-Cuif L, Strähle U. 2010. Heterogeneity in progenitor cell subtypes in the ventricular zone of the zebrafish adult telencephalon. *Glia* **58**:870–888. doi:10.1002/glia.20971

Mathuru AS, Kibat C, Cheong WF, Shui G, Wenk MR, Friedrich RW, Jesuthasan S. 2012. Chondroitin fragments are odorants that trigger fear behavior in fish. *Curr Biol* **22**:538–544. doi:10.1016/j.cub.2012.01.061

Mathys H, Adaikkan C, Gao F, Young JZ, Manet E, Hemberg M, De Jager PL, Ransohoff RM, Regev A, Tsai LH. 2017. Temporal Tracking of Microglia Activation in Neurodegeneration at Single-Cell Resolution. *Cell Rep* **21**:366–380. doi:10.1016/j.celrep.2017.09.039

Maximino C, Meinerz DL, Fontana BD, Mezzomo NJ, Stefanello F V., de S. Prestes A, Batista CB, Rubin MA, Barbosa N V., Rocha JBT, Lima MG, Rosemberg DB. 2018. Extending the analysis of zebrafish behavioral endophenotypes for modeling psychiatric disorders: Fear conditioning to conspecific alarm response. *Behav Processes* **149**:35–42. doi:10.1016/j.beproc.2018.01.020

Mizoguchi T, Fukada M, Iihama M, Song X, Fukagawa S, Kuwabara S, Omaru S, Higashijima SI, Itoh M. 2020. Transient activation of the Notch-her15.1 axis plays an important role in the maturation of V2b interneurons. *Development* **147**:dev191312. doi:10.1242/dev.191312

Mori I, Goshima F, Imai Y, Kohsaka S, Sugiyama T, Yoshida T, Yokochi T, Nishiyama Y, Kimura Y. 2002. Olfactory receptor neurons prevent disseminations of neurovirulent influenza A virus into the brain by undergoing virus-induced apoptosis. *J Gen Virol* **83**:2109–2116. doi:10.1099/0022-1317-83-9-2109

Morikawa H, Sakaguchi S. 2014. Genetic and epigenetic basis of Treg cell development and function: From a FoxP3-centered view to an epigenome-defined view of natural Treg cells. *Immunol Rev* **259**:192–205. doi:10.1111/imr.12174

Moseman EA, Blanchard AC, Nayak D, McGavern DB. 2020. T cell engagement of cross-presenting microglia protects the brain from a nasal virus infection. *Sci Immunol* **5**.

doi:10.1126/sciimmunol.abb1817

Nagayama S, Homma R, Imamura F. 2014. Neuronal organization of olfactory bulb circuits. *Front Neural Circuits* **8**:10.3389. doi:10.3389/fncir.2014.00098

Nässel DR, Zandawala M, Kawada T, Satake H. 2019. Tachykinins: Neuropeptides That Are Ancient, Diverse, Widespread and Functionally Pleiotropic. *Front Neurosci* **13**:1262. doi:10.3389/fnins.2019.01262

Ogawa S, Ramadasan PN, Goschorska M, Anantharajah A, Ng KW, Parhar IS. 2012. Cloning and expression of tachykinins and their association with kisspeptins in the brains of zebrafish. *J Comp Neurol* **520**:2991–3012. doi:10.1002/cne.23103

Olsson T, Kristensson K, Ljungdahl A, Maehlen J, Holmdahl R, Klareskog L. 1989. Gamma-interferon-like immunoreactivity in axotomized rat motor neurons. *J Neurosci* **9**:3870–3875. doi:10.1523/jneurosci.09-11-03870.1989

Oosterhof N, Kuil LE, van der Linde HC, Burm SM, Berdowski W, van Ijcken WFJ, van Swieten JC, Hol EM, Verheijen MHG, van Ham TJ. 2018. Colony-Stimulating Factor 1 Receptor (CSF1R) Regulates Microglia Density and Distribution, but Not Microglia Differentiation In Vivo. *Cell Rep* **24**:1203–1217. doi:10.1016/j.celrep.2018.06.113

Padilla-Coreano N, Bolkan SS, Pierce GM, Blackman DR, Hardin WD, Garcia-Garcia AL, Spellman TJ, Gordon JA. 2016. Direct Ventral Hippocampal-Prefrontal Input Is Required for Anxiety-Related Neural Activity and Behavior. *Neuron* **89**:857–866. doi:10.1016/j.neuron.2016.01.011

Padilla-Coreano N, Canetta S, Mikofsky RM, Alway E, Passecker J, Myroshnychenko M V., Garcia-Garcia AL, Warren R, Teboul E, Blackman DR, Morton MP, Hupalo S, Tye KM, Kellendonk C, Kupferschmidt DA, Gordon JA. 2019. Hippocampal-Prefrontal Theta

Transmission Regulates Avoidance Behavior. *Neuron* **104**:601-610.e4. doi:10.1016/j.neuron.2019.08.006

Pereira L, Medina R, Baena M, Planas AM, Pozas E. 2015. IFN gamma regulates proliferation and neuronal differentiation by STAT1 in adult SVZ niche. *Front Cell Neurosci* **9**:270. doi:10.3389/fncel.2015.00270

Peretto P, Dati C, De Marchis S, Kim HH, Ukhanova M, Fasolo A, Margolis FL. 2004. Expression of the secreted factors noggin and bone morphogenetic proteins in the subependymal layer and olfactory bulb of the adult mouse brain. *Neuroscience* **128**:685–696. doi:10.1016/j.neuroscience.2004.06.053

Pinho-ribeiro FA, Deng L, Neel D V, Erdogan O, Basu H, Yang D, Choi S, Walker AJ, Carneiro-nascimento S, He K, Wu G, Stevens B, Doran KS, Levy D, Chiu IM. 2023. Bacteria hijack a meningeal neuroimmune axis to facilitate brain invasion. *Nature*. doi:10.1038/s41586-023-05753-x

Pinho-Ribeiro FA, Verri WA, Chiu IM. 2017. Nociceptor Sensory Neuron–Immune Interactions in Pain and Inflammation. *Trends Immunol* **38**:5–19. doi:10.1016/j.it.2016.10.001

Pita L, Hoeppner MP, Ribes M, Hentschel U. 2018. Differential expression of immune receptors in two marine sponges upon exposure to microbial-associated molecular patterns. *Sci Rep* **8**:16081. doi:10.1038/s41598-018-34330-w

Plachez C, Cato K, McLeay RC, Heng YHE, Bailey TL, Gronostajski RM, Richards LJ, Puche AC, Piper M. 2012. Expression of nuclear factor one A and -B in the olfactory bulb. *J Comp Neurol* **520**:3135–3149. doi:10.1002/cne.23081

Quarta A, Berneman Z, Ponsaerts P. 2020. Neuroprotective modulation of microglia effector functions following priming with interleukin 4 and 13: current limitations in understanding

their mode-of-action. *Brain Behav Immun* **88**:856–866. doi:10.1016/j.bbi.2020.03.023

Rieskamp JD, Denninger JK, Dause TJ. 2018. Identifying the unique role of notch3 in adult neural stem cell maintenance. *J Neurosci* **38**:3157–3159. doi:10.1523/JNEUROSCI.3531-17.2018

Rivera AS, Ozturk N, Fahey B, Plachetzki DC, Degnan BM, Sancar A, Oakley TH. 2012. Blue-light-receptive cryptochrome is expressed in a sponge eye lacking neurons and opsin. *J Exp Biol* **215**:1278–1286. doi:10.1242/jeb.067140

Rodgers JT, King KY, Brett JO, Cromie MJ, Charville GW, Maguire KK, Brunson C, Mastey N, Liu L, Tsai CR, Goodell MA, Rando TA. 2014. mTORC1 controls the adaptive transition of quiescent stem cells from G0 to GAlert. *Nature* **510**:393–396. doi:10.1038/nature13255

Salesse R, Baly C, Negroni J, Meunier N, Caillol M, Congar P. 2012. Neuropeptide Y Enhances Olfactory Mucosa Responses to Odorant in Hungry Rats. *PLoS One* **7**:e45266. doi:10.1371/journal.pone.0045266

Schmidt R, Strähle U, Scholpp S. 2013. Neurogenesis in zebrafish - from embryo to adult. *Neural Dev* **8**. doi:10.1186/1749-8104-8-3

Schubert M, Brazil DP, Burks DJ, Kushner JA, Ye J, Flint CL, Farhang-Fallah J, Dikkes P, Warot XM, Rio C, Corfas G, White MF. 2003. Insulin receptor substrate-2 deficiency impairs brain growth and promotes tau phosphorylation. *J Neurosci* **23**:7084–7092. doi:10.1523/jneurosci.23-18-07084.2003

Sebastián-Serrano A, Sandonis A, Cardozo M, Rodríguez-Tornos FM, Bovolenta P, Nieto M. 2012. Pαx6 expression in postmitotic neurons mediates the growth of axons in response to SFRP1. *PLoS One* **7**:e31590. doi:10.1371/journal.pone.0031590

Semple SL, Rodríguez-Ramos T, Carpio Y, Lumsden JS, Estrada MP, Dixon B. 2019. PACAP is

lethal to flavobacterium psychrophilum through either direct membrane permeabilization or indirectly, by priming the immune response in rainbow trout macrophages. *Front Immunol* **10**:926. doi:10.3389/fimmu.2019.00926

Sepahi A, Kraus A, Casadei E, Johnston CA, Galindo-villegas J, Kelly C, García-Morenoc D, Muñoze P, Mulero V, Huertas M, Salinas I. 2019. Olfactory sensory neurons mediate ultrarapid antiviral immune responses in a TrkA-dependent manner. *PNAS* **116**:12428–12436. doi:10.1073/pnas.1900083116

Shimada T, Sugiura H, Yamagata K. 2013. Neuritin: A therapeutic candidate for promoting axonal regeneration. *World J Neurol* **3**:138–143. doi:10.5316/wjn.v3.i4.138

Shimada T, Yoshida T, Yamagata K. 2016. Neuritin mediates activity-dependent axonal branch formation in part via FGF signaling. *J Neurosci* **36**:4534–4548. doi:10.1523/JNEUROSCI.1715-15.2016

Silva NJ, Dorman LC, Vainchtein ID, Horneck NC, Molofsky A V. 2021. In situ and transcriptomic identification of microglia in synapse-rich regions of the developing zebrafish brain. *Nat Commun* **12**:5916. doi:10.1038/s41467-021-26206-x

Song E, Zhang C, Israelow B, Lu-Culligan A, Prado AV, Skriabine S, Lu P, Weizman O El, Liu F, Dai Y, Szigeti-Buck K, Yasumoto Y, Wang G, Castaldi C, Heltke J, Ng E, Wheeler J, Alfajaro MM, Levavasseur E, Fontes B, Ravindra NG, van Dijk D, Mane S, Gunel M, Ring A, Jaffar Kazmi SA, Zhang K, Wilen CB, Horvath TL, Plu I, Haik S, Thomas JL, Louvi A, Farhadian SF, Huttner A, Seilhean D, Renier N, Bilguvar K, Iwasaki A. 2021. Neuroinvasion of SARS-CoV-2 in human and mouse brain. *J Exp Med* **218**:e20202135. doi:10.1084/JEM.20202135

Stewart AM, Braubach O, Spitsbergen J, Gerlai R, Kalueff A V. 2014. Zebrafish models for

translational neuroscience research: From tank to bedside. *Trends Neurosci* **37**:264–278. doi:10.1016/j.tins.2014.02.011

Takada N, Kucenas S, Appel B. 2010. Sox10 is necessary for oligodendrocyte survival following axon wrapping. *Glia* **58**:996–1006. doi:10.1002/glia.20981

Tepe B, Hill MC, Pekarek BT, Hunt PJ, Martin TJ, Martin JF, Arenkiel BR. 2018. Single-Cell RNA-Seq of Mouse Olfactory Bulb Reveals Cellular Heterogeneity and Activity-Dependent Molecular Census of Adult-Born Neurons. *Cell Rep* **25**:2689-2703.e3. doi:10.1016/j.celrep.2018.11.034

Tiveron MC, Beclin C, Murgan S, Wild S, Angelova A, Marc J, Coré N, de Chevigny A, Herrera E, Bosio A, Bertrand V, Cremer H. 2017. Zic-proteins are repressors of dopaminergic forebrain fate in mice and C. Elegans. *J Neurosci* **37**:10611–10623. doi:10.1523/JNEUROSCI.3888-16.2017

Torres-Fernández O, Santamaría-Romero G, Hurtado AP, Monroy-Gómez J, Daza NA. 2018. Entry of Rabies Virus in the Olfactory Bulb of Mice and Effect of Infection on Cell Markers of Neurons and Astrocytes. *Int J Morphol* **36**:670–676. doi:10.4067/s0717-95022018000200670

van den Pol AN, Ding S, Robek MD. 2014. Long-Distance Interferon Signaling within the Brain Blocks Virus Spread. *J Virol* **88**:3695–3704. doi:10.1128/jvi.03509-13

Van Der Kallen LR, Eggers R, Ehlert EM, Verhaagen J, Smit AB, Van Kesteren RE. 2015. Genetic deletion of the transcriptional repressor NFIL3 enhances axon growth in vitro but not axonal repair in vivo. *PLoS One* **10**:e0127163. doi:10.1371/journal.pone.0127163

van der Linden CJ, Gupta P, Bhuiya AI, Riddick KR, Hossain K, Santoro SW. 2020. Olfactory Stimulation Regulates the Birth of Neurons That Express Specific Odorant Receptors. *Cell*

Rep **33**:108210. doi:10.1016/j.celrep.2020.108210

Van Riel D, Verdijk R, Kuiken T. 2015. The olfactory nerve: A shortcut for influenza and other viral diseases into the central nervous system. *J Pathol* **235**:277–287. doi:10.1002/path.4461

Varoqueaux F, Williams EA, Grandemange S, Truscello L, Kamm K, Schierwater B, Jékely G, Fasshauer D. 2018. High Cell Diversity and Complex Peptidergic Signaling Underlie Placozoan Behavior. *Curr Biol* **28**:3495-3501.e2. doi:10.1016/j.cub.2018.08.067

Wei S, Zhou JM, Chen X, Shah RN, Liu J, Orcutt TM, Traver D, Djeu JY, Litman GW, Yoder JA. 2007. The zebrafish activating immune receptor Nitr9 signals via Dap12. *Immunogenetics* **59**:813–821. doi:10.1007/s00251-007-0250-6

West AP, Shadel GS, Ghosh S. 2011. Mitochondria in innate immune responses. *Nat Rev Immunol* **11**:389–402. doi:10.1038/nri2975

Wheeler DL, Athmer J, Meyerholz DK, Perlman S. 2017. Murine Olfactory Bulb Interneurons Survive Infection with a Neurotropic Coronavirus. *J Virol* **91**:01099–17. doi:10.1128/jvi.01099-17

Wu S, Nguyen LTM, Pan H, Hassan S, Dai Y, Xu J, Wen Z. 2020. Two phenotypically and functionally distinct microglial populations in adult zebrafish. *Sci Adv* **6**:eabd1160. doi:10.1126/sciadv.abd1160

Zeppilli S, Ackels T, Attey R, Klimpert N, Ritola KD, Boeing S, Crombach A, Schaefer AT, Fleischmann A. 2021. Molecular characterization of projection neuron subtypes in the mouse olfactory bulb. *Elife* **10**:e65445. doi:10.7554/eLife.65445

Zheng G qing, Li Y, Gu Y, Chen X miao, Zhou Y, Zhao S zhi, Shen J. 2010. Beyond water channel: Aquaporin-4 in adult neurogenesis. *Neurochem Int* **56**:651–654. doi:10.1016/j.neuint.2010.01.014

Zhou Y, Zhou B, Pache L, Chang M, Khodabakhshi AH, Tanaseichuk O, Benner C, Chanda SK. 2019. Metascape provides a biologist-oriented resource for the analysis of systems-level datasets. *Nat Commun* **10**. doi:10.1038/s41467-019-09234-6

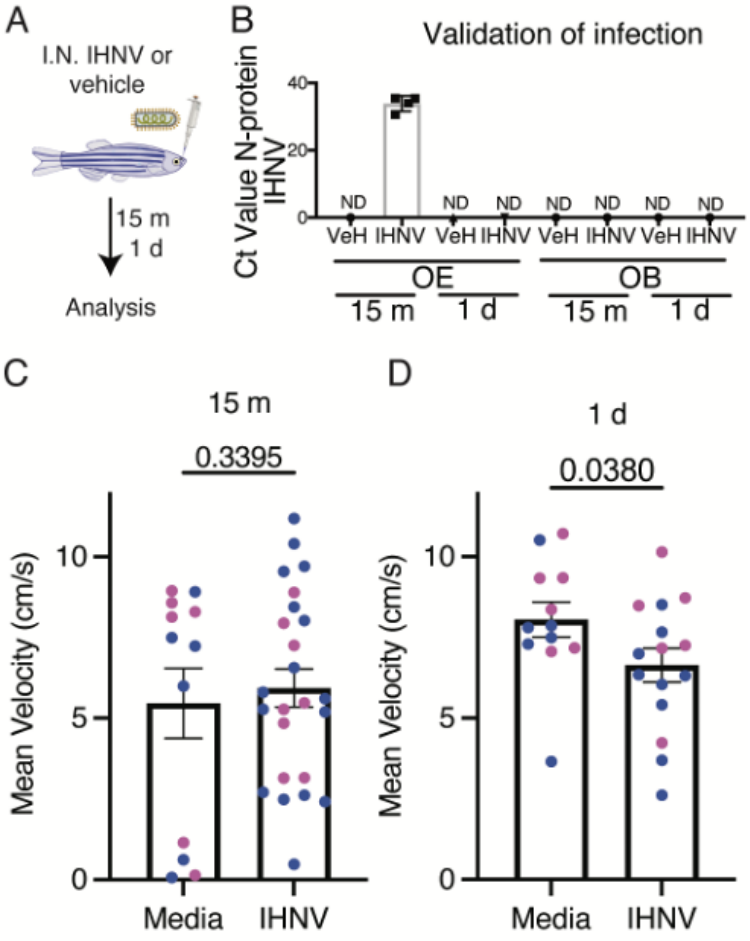

Figure 1. Without viral translocation to the brain I.N. IHNV changes adult behavior at 1 d. (A) schematic of intranasal administration of aquatic rhabdovirus infectious hematopoietic necrosis virus (IHNV) or vehicle (VeH). (B) quantification of IHNV N-protein presence in the olfactory organ and olfactory bulb 15 m and 1 d after I.N. delivery of virus. N = 4-6, each replicate is a pool of 4 animals. (C) Average velocity of the animal over the test for 15 m (C) or 1 d (D) after IHNV or media control. Test was run for 5 m after IHNV or control odorant was

added to the flow cell. Statistics are Student's T test. Error bars are SEM. Male (blue) and female (pink) animals do not show a difference in behavior.

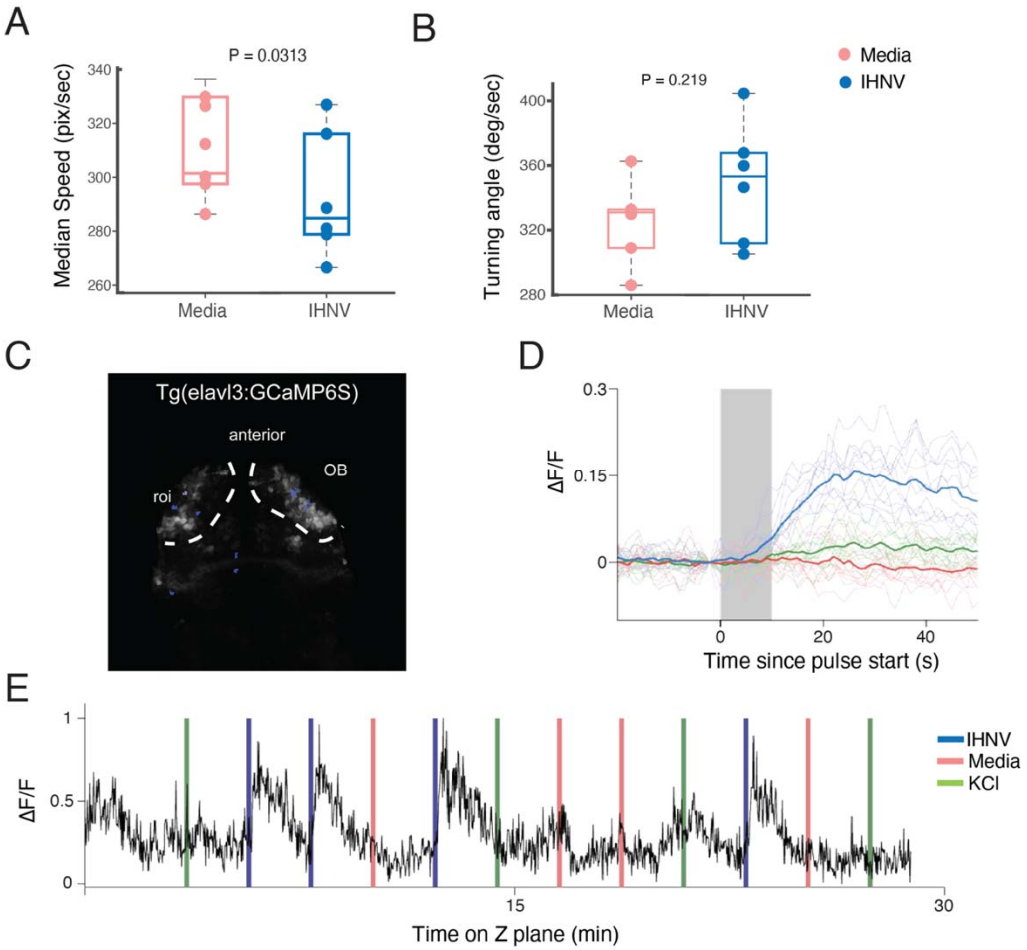

Figure 2. Neuronal activation of the zebrafish OO and OB in response to nasal viral delivery. (A) Median speed of larva in a lateral flow chamber exposed to IHNV for 4 seconds. Speed adjusted for the flow rate. (B) Turning angle of larval zebrafish in lateral flow cell. Test was run for 5 m after IHNV or control odorant was added to the flow cell. Statistics are Student's T test. (C) Maximum intensity projection of olfactory system of a Tg(elavl3:GCaMP6S) larva imaged by 2-P microscopy. Odorants were applied to the olfactory pit randomly every 2 minutes and animals imaged for 6 h., OB = olfactory bulb. Indicated in blue are ROIs activated by to IHNV virus but do not respond to the other stimuli. (D) Stimulus triggered average changes in fluorescence (F/F_0) following each stimulus (indicated by color) for cells that show showing neuronal activation specific to the IHNV (red) and not the positive (KCl, green) or negative

(Media, blue) controls. Mean response across IHNV-selective cells is indicated in bold. (E) F/F_0 traces of the highlighted ROI in C. Vertical lines color coding indicates the type of stimuli delivered at each interval.

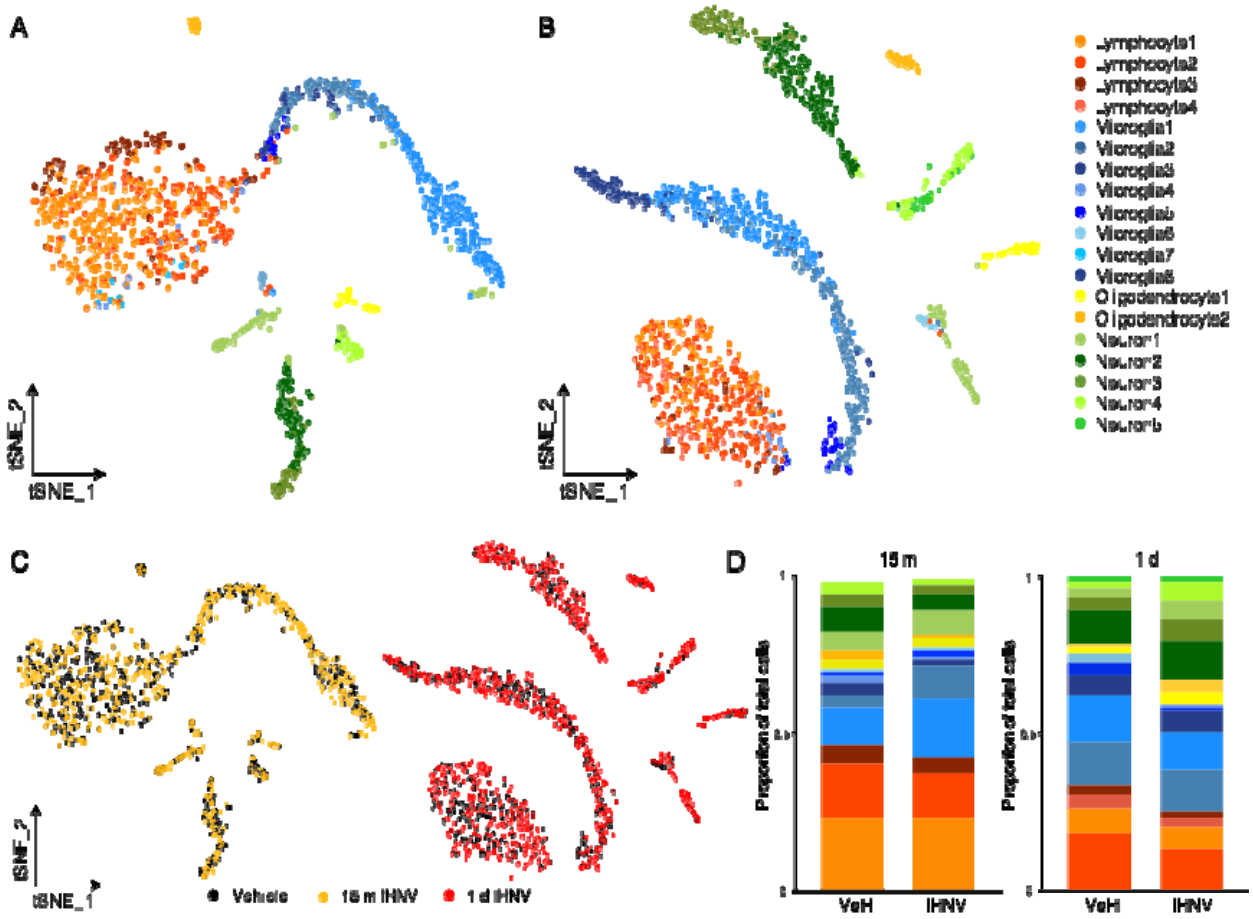

Figure 3. sc-RNA seq of the olfactory bulb reveals changes to the cellular landscape after I.N. IHNV. tSNE plots of single cells isolated from the olfactory bulb at 15 m (A) and 1 d (B). (C) tSNE plots showing Vehicle (VeH) (black), 15 m IHNV (yellow), and 1 d IHNV (red). (D) Bar plots of proportions of cells from each cluster for each treatment. Statistical proportional analysis for changes to the proportions following IHNV treatment is in supplemental figure X.

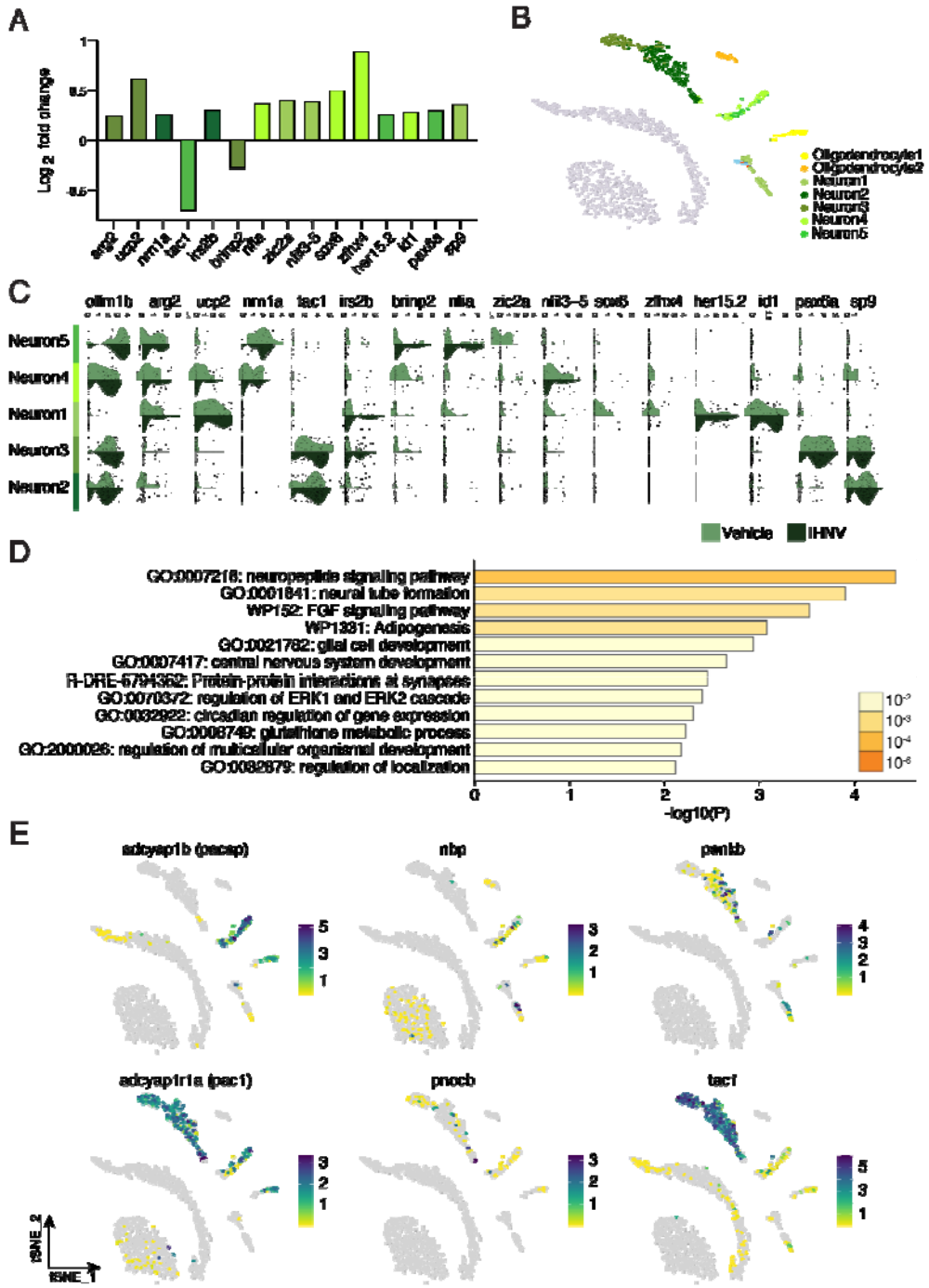

Figure 4. Transcriptional profiles of neurons reveal increased development at 1 d after intranasal delivery of virus. (A) Bar plots showing fold change expression of significantly differentially expressed genes in neurons 1 d after I.N. IHNV relative to control. Bars are colored

according to the cluster in which they are differentially expressed. (B) tSNE highlighting only the neuronal clusters (C) violin plots of differentially expressed genes in neuronal clusters 1 d after intranasal IHNV delivery shows many genes related to plasticity and development of neurons are upregulated compared to vehicle treated animals. (C) gene ontology of all differentially expressed genes in neuronal clusters 1 d I.N. IHNV compared to 1 d I.N. vehicle treatment. Gene ontology was run on Metascape (Zhou et al., 2019).(E) Feature plots for genes enriched in the top GO:0007218 Neuropeptide signaling pathway (*pacap*, *npb*, *penkb*, *scg5*, and *tac1*) and pacap receptor *pac1*.

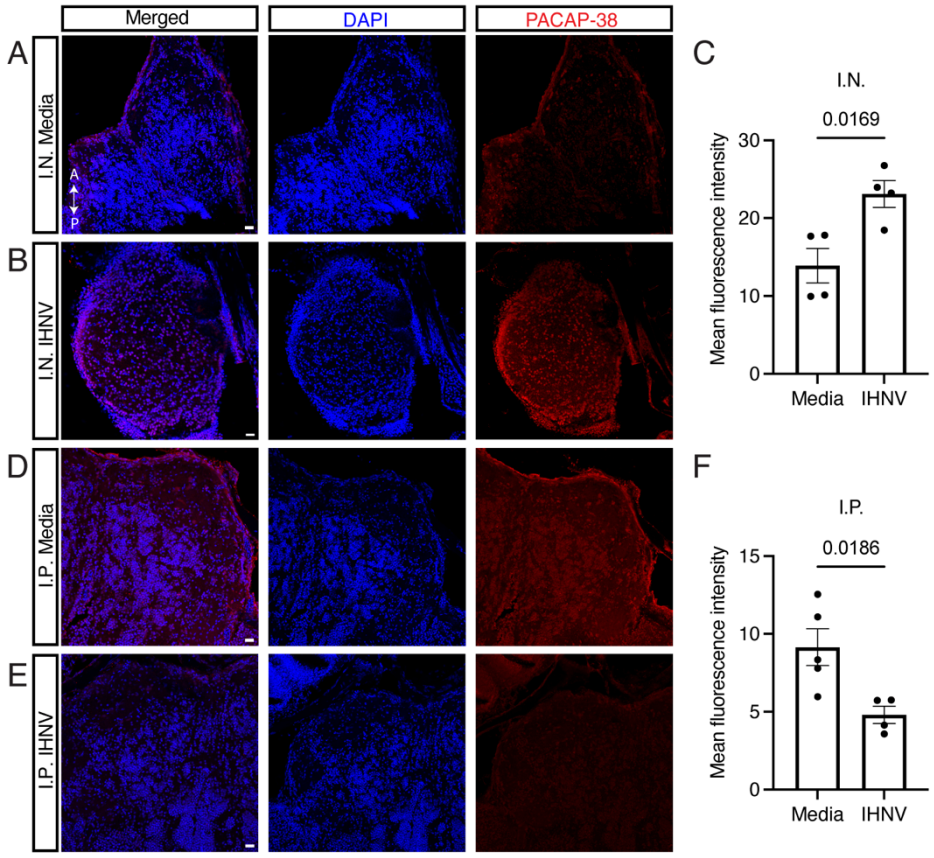

Figure 5: Neuropeptide PACAP-38 expression increases in the zebrafish OB 1 d after I.N. IHNV but not 1 d after I.P. IHNV treatment. (A) Representative confocal image of the zebrafish OB stained with anti-PACAP-38 antibody after receiving vehicle by I.N. delivery. (B) Representative confocal image of the zebrafish OB stained with anti-PACAP-38 antibody after receiving IHNV by I.N. delivery. (C) Quantification of the mean fluorescent intensity values for A and B. (D) Representative confocal image of the zebrafish OB stained with anti-PACAP-38 antibody after receiving vehicle by I.P. delivery. (E) Representative confocal image of the zebrafish OB stained with anti-PACAP-38 antibody after receiving IHNV by I.P. delivery. (F) Quantification of the mean fluorescent intensity values for D and E. P-values were calculated by a student's T test, with error bars indicating standard error of the mean.

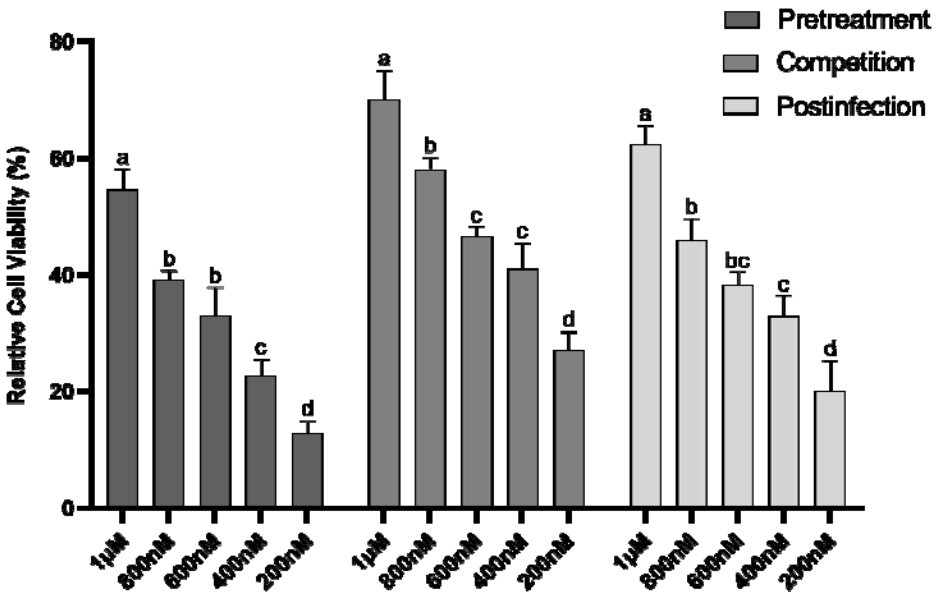

Figure 6. Amidated PACAP-96% protects EPC cells from IHNV-induced cell death. Relative percent viability of EPC cells that were either pretreated with amidated PACAP-38 prior to infection (pretreatment), treated with amidated PACAP-38 at the time of the infection (competition) or infected with IHNV and then treated with different concentrations of amidated PACAP-38 (postinfection). Results are representative of two independent experiments with N=4 for each treatment group. Different letters indicate significant differences among treatments by one-way ANOVA ($P<0.05$).

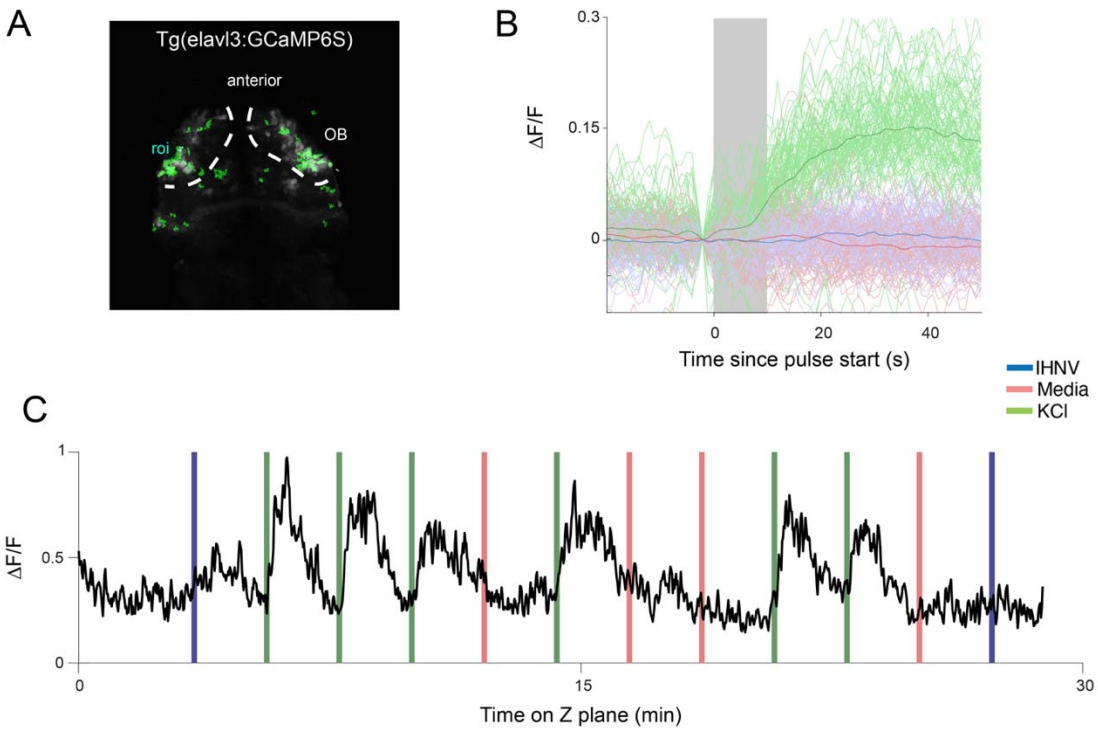

Supplemental Figure 1: (A) Olfactory system of a Tg(elavl3:GCaMP6S) larva imaged by 2-P microscopy. Odorants were applied to the olfactory pit randomly every 2 minutes and animals imaged for 6 h., OB = olfactory bulb. Indicated in green are ROIs selective to KCl that do not respond to the other stimuli. (B) Stimulus triggered average changes in fluorescence (F/F_0) following each stimulus for cells that show neuronal activation specific to the positive (KCl) control (green line) but not the IHNV (red line) virus or negative control (Media, blue line). Mean response across KCl-selective cells. (C) F/F_0 traces of the highlighted ROI in A. Vertical lines color coding indicates the type of stimuli delivered at each interval.

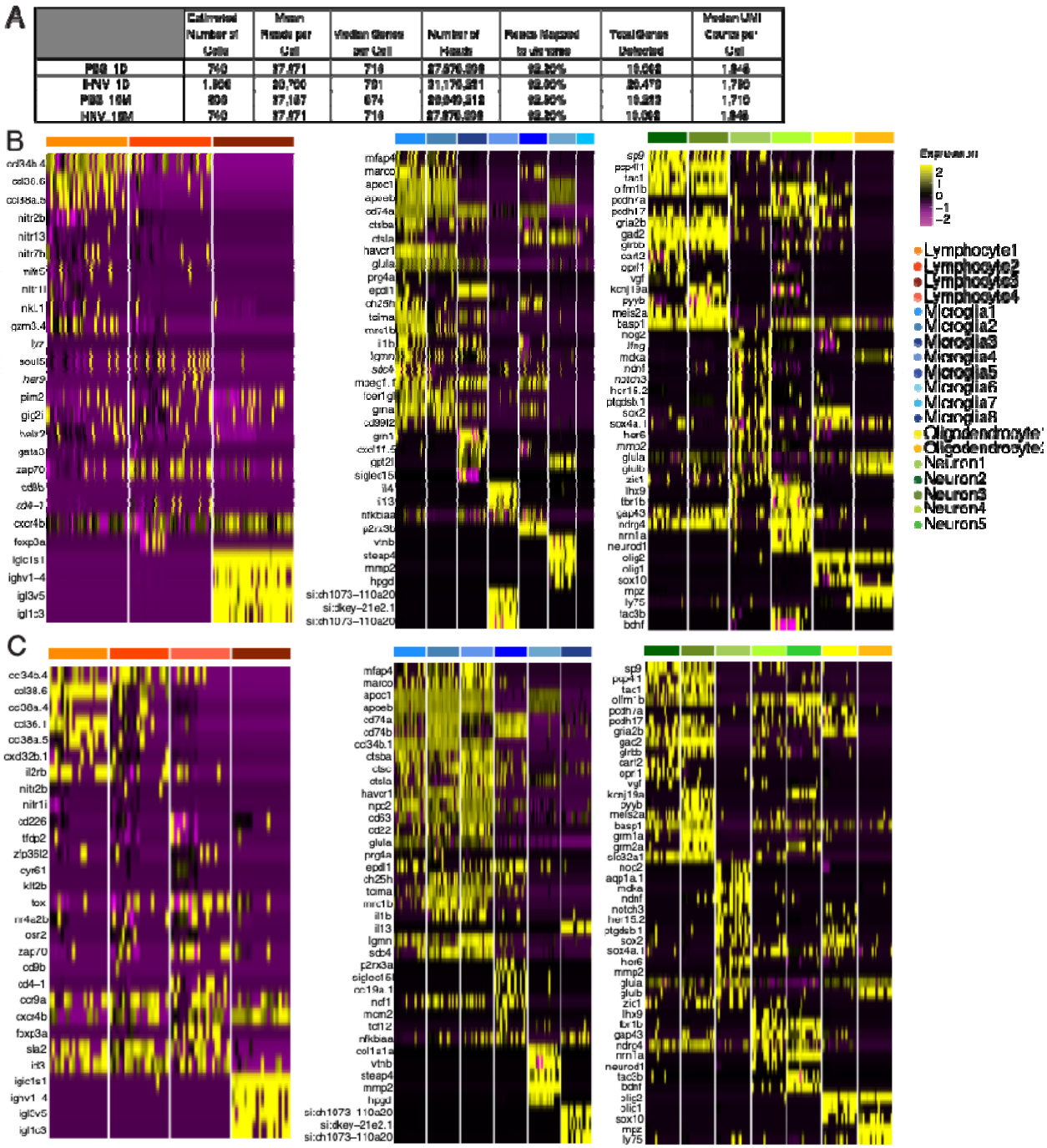

Supplemental Figure 2. Transcriptional landscape of the adult zebrafish olfactory bulb 15 m and 1 d after intranasal viral delivery. (A) Metrics from each sample collected by 10x Genomics Chromium platform after sequencing on Illumina MiSeq. (B) Heat map of cluster

markers for lymphocyte, microglial, and neuronal clusters from CCA integrated Vehicle and IHNV treated cells from the olfactory bulb 15 m after intranasal treatment. (C) Heat map of cluster markers for lymphocyte, microglial, and neuronal clusters from CCA integrated Vehicle and IHNV treated cells from the olfactory bulb 1 d after intranasal treatment.

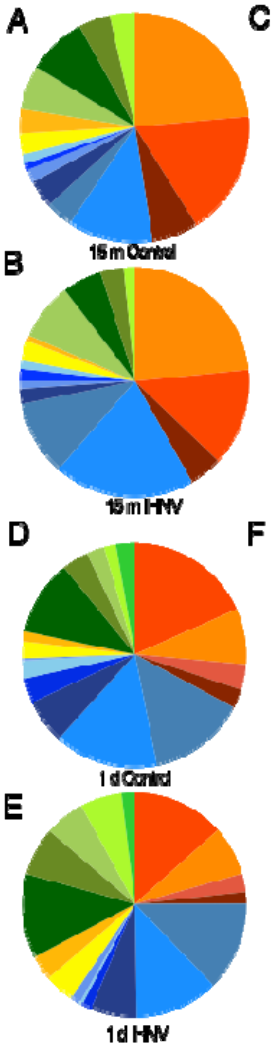

C

15 m	# cells Control	# cells Treatment	Control prop	Treatemnt prop	# cells Control Normalized	Bonferroni P.adj
Lymphocyte1	169	177	0.29	0.23	179	1
Lymphocyte2	121	104	0.17	0.14	133	0.851
Lymphocyte3	46	36	0.06	0.05	49	1
Microglia1	82	148	0.12	0.19	90	0.002
Microglia2	26	79	0.04	0.10	29	0.00003
Microglia3	26	16	0.04	0.02	29	1
Microglia4	13	8	0.02	0.01	14	1
Microglia5	6	13	0.01	0.02	7	1
Microglia6	9	9	0.01	0.01	10	1
Oligodendrocyte1	20	21	0.03	0.03	22	1
Oligodendrocyte2	24	8	0.03	0.01	26	0.011
Neuron1	43	61	0.06	0.08	47	1
Neuron2	57	42	0.08	0.05	63	0.825
Neuron3	31	25	0.04	0.03	34	1
Neuron4	25	12	0.04	0.02	27	0.350

F

1 d	# cells Control	# cells Treatment	Control prop	Treatemnt prop	# cells Control Normalized	Bonferroni P.adj
Lymphocyte2	116	197	0.18	0.13	229	0.101
Lymphocyte1	51	90	0.08	0.07	101	1
Lymphocyt4	23	33	0.04	0.03	48	1
Lymphocyte3	17	21	0.03	0.02	34	1
Microglia2	88	180	0.14	0.13	175	1
Microglia1	93	149	0.15	0.12	185	1
Microglia8	40	82	0.06	0.07	79	1
Microglia5	22	17	0.04	0.01	44	0.064
Microglia6	16	5	0.03	0.00	32	0.001
Microglia4	2	17	0.00	0.01	4	1
Oligodendrocyte1	15	53	0.02	0.04	30	0.973
Oligodendrocyte2	9	44	0.01	0.04	18	0.954
Neuron2	68	150	0.11	0.12	135	1
Neuron3	24	87	0.04	0.07	48	0.147
Neuron1	16	72	0.03	0.06	32	0.048
Neuron4	11	75	0.02	0.06	22	0.001
Neuron5	17	24	0.03	0.02	34	1

Supplemental Figure 3. Cellular landscape of the olfactory bulb 15 m and 1 d after intranasal delivery of vehicle (PBS) and virus. (A&B) proportional analysis of cells in each cluster in each treatment for 15 m with statistical analysis in (C). (D&E) proportions analysis of cells in each cluster in each treatment for 15 m with statistical analysis in (F) When the *P*-value<0.05, the null hypothesis that population sizes are the same in both treatment groups is rejected.

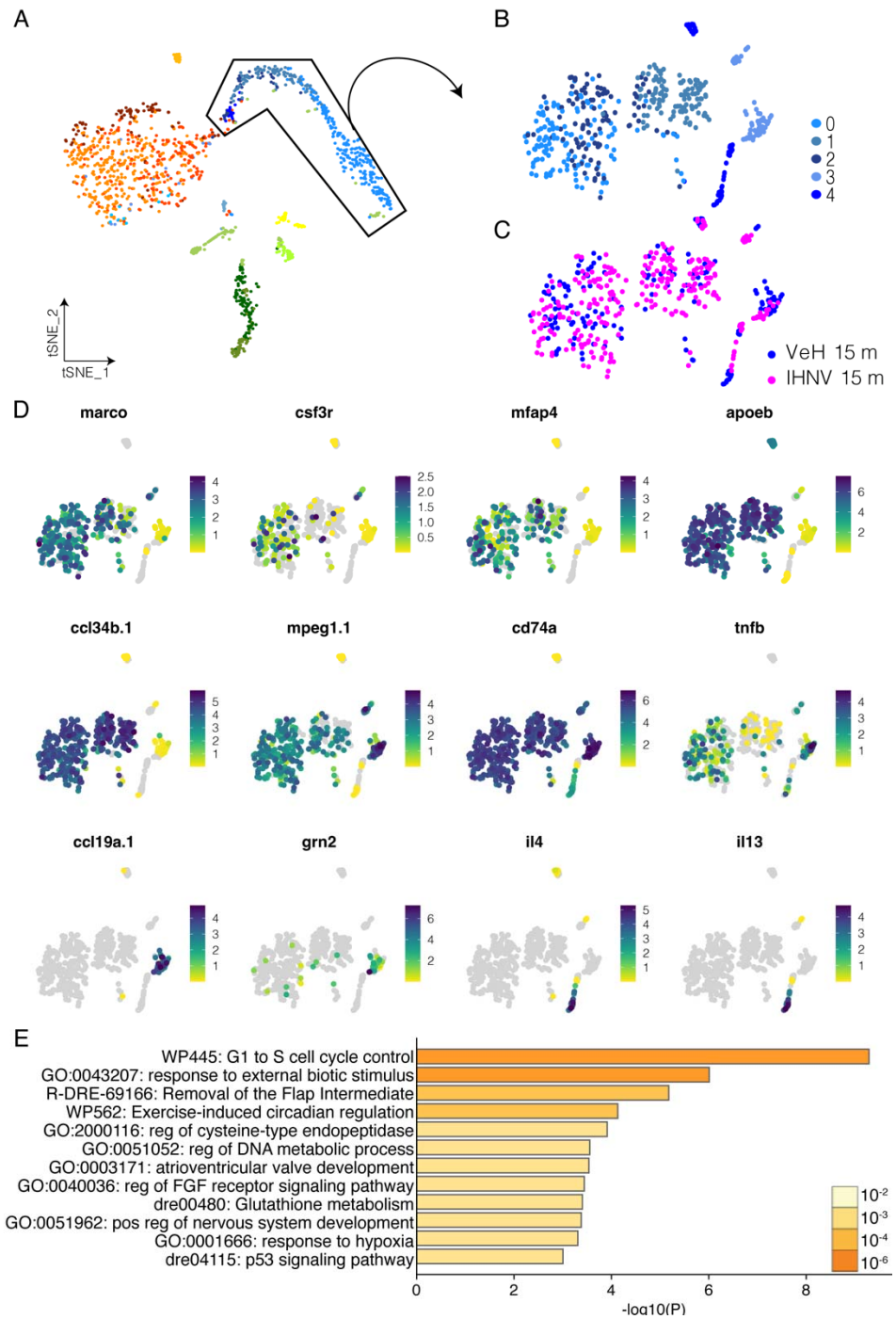

Supplemental Figure 4. Microglia and macrophage populations in the adult zebrafish OB are diverse. (A) tSNE of the whole OB 15 m after I.N. IHNV to represent the microglial cell types that were subclustered in (B) and represented as either vehicle (VeH) control (blue) or IHNV treated (pink) (C). (D) Feature plots showing markers of microglia (*marco, csf3r, mfap,*

apoeb) and ameboid like microglia (*ccl34b.1)* as well as macrophages (*mpeg1.1, ccl19a.1, grn2).* (E) Gene ontology of differentially regulated genes from microglial clusters 15 min after I.N. IHNV compared to vehicle. Gene ontology was run on Metascape (Zhou et al., 2019).

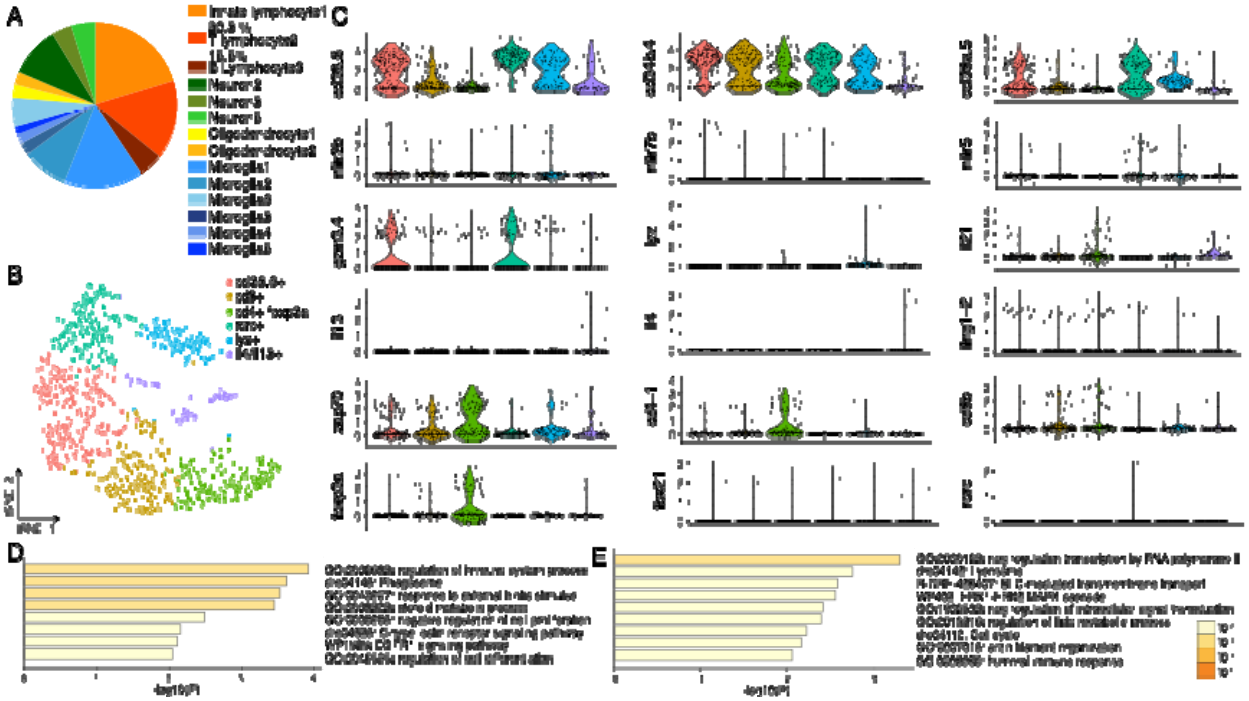

Supplemental Figure 5. Diverse lymphocyte clusters are found in the adult zebrafish OB. (A) Proportions of clusters from figure 6 of only control cells shows innate-like lymphocytes are 20% of cells captured from the control olfactory bulb and T lymphocytes2 are 15% of cells captured from the control olfactory bulb. (B) t-SNE of innate/T lymphocyte subsets from the olfactory bulb show 6 unique phenotypes. (C) Violin plots of markers of natural killer (*ccl38.6, ccl34b.4, ccl38a.5, nitr*), cytotoxic (*gzm3.4, lyz, ifng1-2, tbx21*), type II innate-like lymphocytes (*il13, il4*), type III innate like lymphocytes (*il2, rorc*) and Tregs (*foxp3a, cd4)*. (D) Gene ontology of significantly differentially expressed genes from lymphocytes in the olfactory bulb 15 m after I.N. IHNV compared to 1d I.N. vehicle treated lymphocytes. (E) Gene ontology of significantly differentially expressed genes from lymphocytes in the olfactory bulb 1 d after I.N. IHNV compared to 1d I.N. vehicle treated lymphocytes. Gene ontology was run on Metascape (Zhou et al., 2019).

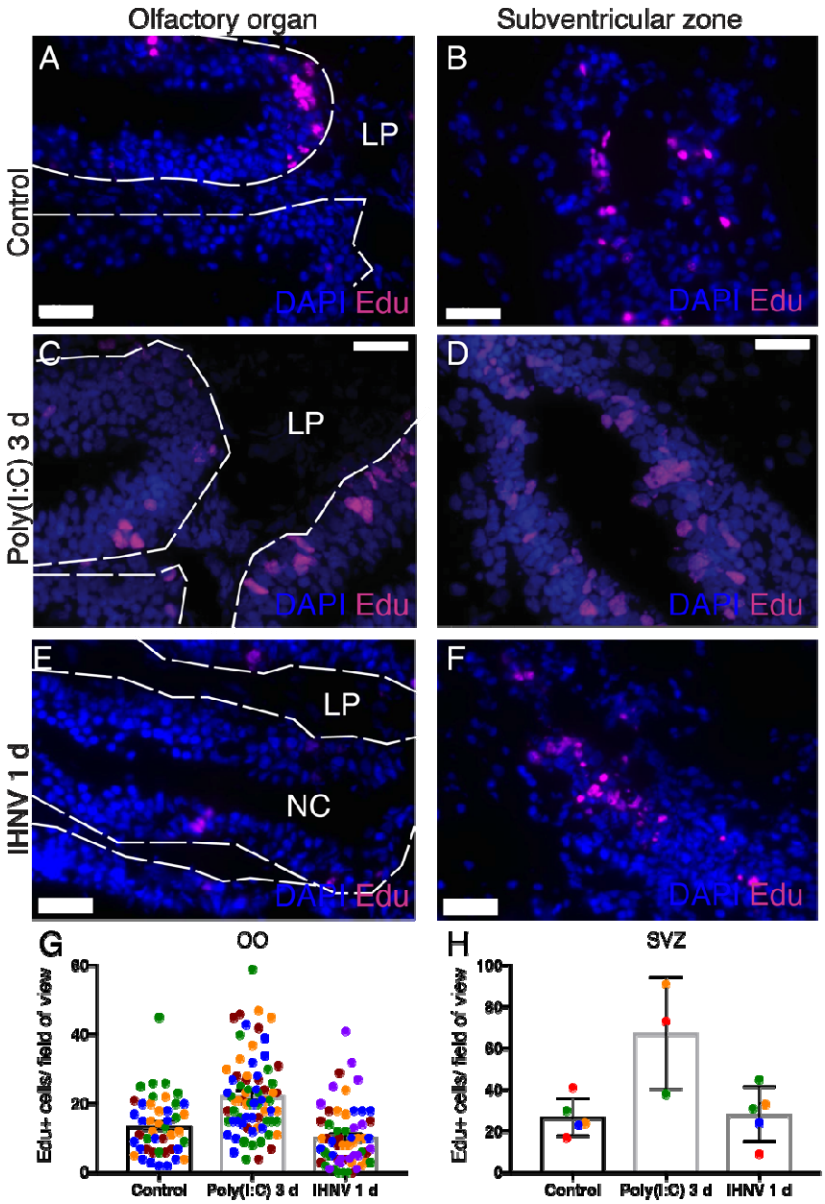

Supplemental Figure 6. I.N. IHNV does not induce proliferation in the zebrafish olfactory organ or the subventricular zone of the telencephalon. Proliferation detected using Edu (pink) in control (A) 3 d I.N. Poly(I:C) (C) or 1 d I.N. IHNV (E) in the olfactory organ (OO) quantified in (G). Proliferation detected using Edu in control (B) 3 d I.N. Poly(I:C) (D) or 1 d I.N. IHNV (F) in the subventricular zone (SVZ) quantified in (H). scale = 20mm. N= 3-5. Each color indicates a separate animal and each dot a field of view at 60x. Statistics are Student's T test between control and each treatment and not significant for the IHNV treatment.

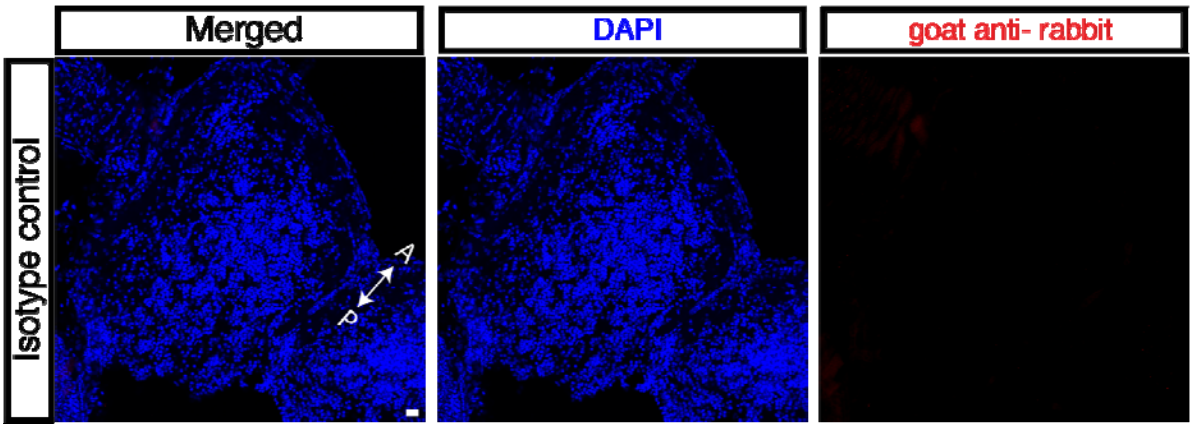

Supplemental Figure 7: Isotype control staining of zebrafish OB cryosections for anti-PACAP-38 staining. Scale bar = 20um.

		%ident
D. rerio	HSDGIFTDIYSRYRKQMAVKKYLAAVLGRRYRQRVKNK	
H. sapiens	HSDGIFTDSYSRYRKQMAVKKYLAAVLGKRYKQRVKNK	89%
C. gariepinus	HSDGIFTDSYSRYRKQMAVKKYLAAVLGRRYRQRFRNK	92%
	******** **********:**:**.:**	

Supplemental Figure 8: Alignment of PACAP-38 sequences from *D. rerio* (NP_001259010.1:96-133), *Homo sapiens* mature PACAP-38 peptide (NP_001093203.1:132-169), and *C. gariepinus* from (Semple et al., 2019). Percent identity is compared to *D. rerio.*

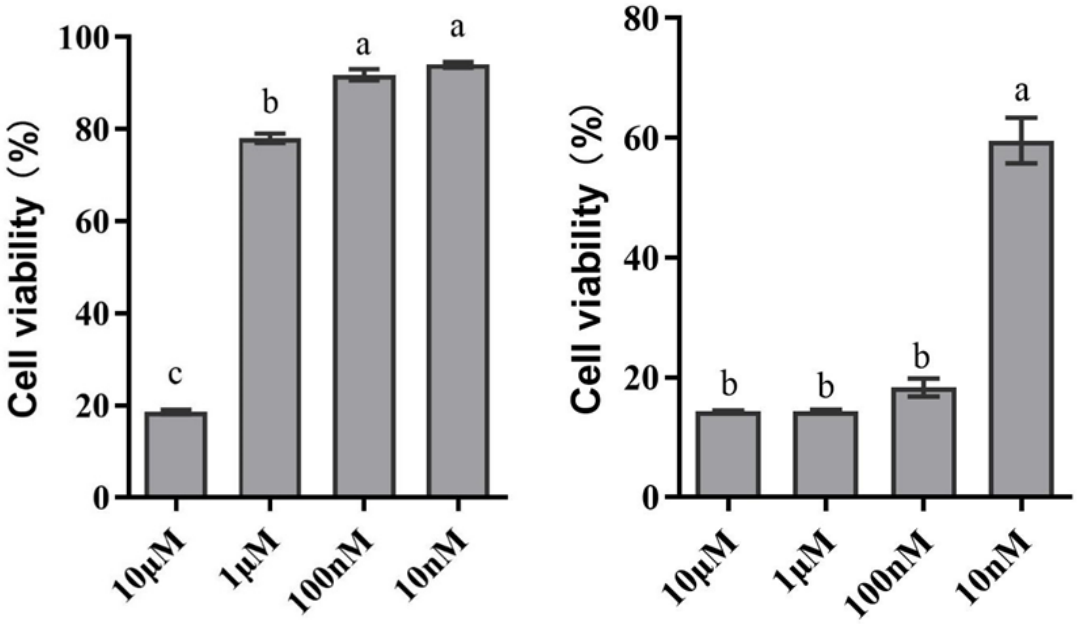

Supplemental Figure 9: Cytotoxicity of PACAP in EPC cells. (Left, amidated PACAP-96%; right, PACAP-85%;). Different letters indicate statistically significant differences by one-way ANOVA. Results are indicative of two independent experiments.

Supplemental Table 1. Enrichment table of the top gene ontology terms and the genes differentially expressed in neurons of the OB at 1 d after I.N. IHNV.

Term	Description	LogP	Genes
GO:0007218	neuropeptide signaling pathway	-4.417804382	adcyap1b, penkb, scg5, pnccb, lac1 npb, grla2b, gabrb2a, lpar1, p2rx3b, galr1b, uts1, sst7, crhbp
GO:0001841	neural tube formation	-3.890903551	dlx6a, zic2a, zic5, ccdc88c
WP152	FGF signaling pathway	-3.513676806	egr2b, etv5b, spry4, egr2a, stf3, sp9, vegfaa, tgfb1a
WP1331	Adipogenesis	-3.065857087	egr2b, lpl, cebpd, tgfb1a, rb1
GO:0021782	glial cell development	-2.924061261	egr2b, prdm8, tuba8l3, ndrg1a, slitrk2
GO:0007417	central nervous system development	-2.643993251	egr2b, etv5b, pax6a, six3a, zic2a, fezf2, spry4, gsna, adcyap1b, zic5, prdm8, sox6, zfhx3b her15.1, lmo2, cd74a, dnajb1b, tgfb1a, slitrk2, taldn1
R-DRE-6794362	Protein-protein interactions at synapses	-2.444273438	caska, homer1b, slitrk2
GO:0070372	regulation of ERK1 and ERK2 cascade	-2.389916214	cd74a, spry4, adcyap1b, ccl44
GO:0032922	circadian regulation of gene expression	-2.295638978	id1, id2b, nfil3-b
GO:0006749	glutathione metabolic process	-2.215221521	clic4, clic2, gpx1b
GO:2000026	regulation of multicellular organismal development	-2.169337426	id1, vegfaa, zic5, egfl6, sox6, scg2b, slitrk2, btbd8a, her15.1, cebpd, nfkbiaa, brinp2, zfhx3b
GO:0032879	regulation of localization	-2.110433392	caska, adcyap1b, clic4, scg5, homer1b, clic2, crhbp, afdna, cnh3, apoc1, fgf12a